Title: Antigen presentation by discrete class I molecules on brain endothelium dynamically regulates T-cell mediated neuropathology in experimental cerebral malaria

[1,5]Fain, CE, [3,5]Zheng, J, [1]Jin, F, [1]Ayasoufi, K, Wu, Y, [5]Lilley, MT, [1,5]Dropik, AR, [1]Wolf, DM, Rodriguez, RC, [4,5]Aibaidula, A, [1,5]Tritz, ZP, [5]Bouchal, SM, [7]Pewe, LL, [7]Urban, SL, [1,5]Chen, Y, [6]Chang, S, [1]Hansen, MJ, [9]Kachergus, JM, [9]Shi, J, [9]Thompson, EA, [7]Harty, JT, [6]Parney, IF, [8]Sun, J, [1,3]Wu, LJ, [1,2,3]Johnson, AJ*

[1] Mayo Clinic Department of Immunology, Rochester, MN
[2] Mayo Clinic Department of Molecular Medicine, Rochester, MN
[3] Mayo Clinic Department of Neurology, Rochester, MN
[4] Mayo Clinic Department of Molecular Pharmacology and Experimental Therapeutics
[5] Mayo Clinic Graduate School of Biomedical Sciences, Rochester, MN
[6]Mayo Clinic Department of Neurosurgery, Rochester, MN
[7]University of Iowa Department of Pathology, Iowa City, IA
[8]University of Virginia Department of Medicine, Charlottesville, VA
[9]Mayo Clinic Department of Cancer Biology, Jacksonville, FL

Authors have no conflicts or competing interests to disclose.

Author contributions: CEF, JZ, FJ, KA, MTL, ARD, DMW, RCR, AA, and ZPT assisted with experiments. CEF, JZ, FJ, YW, SMB, YC, JMK, and JS analyzed data. CEF and AJJ designed experiments and interpreted results. CEF wrote the manuscript. All authors provided feedback for editing, read manuscript, and agree with data presented.

*Correspondence to Aaron J. Johnson, PhD
Professor and Consultant
Departments of Immunology, Neurology, and Molecular Medicine
Guggenheim 4-11C
Mayo Clinic
200 First St. SW
Rochester, MN 55905
Johnson.aaron2@mayo.edu
Tel: (507) 266-1973

Abstract

CD8 T cell engagement of brain vasculature is a putative mechanism of neuropathology in human cerebral malaria. To define contributions of brain endothelial cell MHC class I antigen-presentation to CD8 T cells in establishing this pathology, we developed novel H-2K^b LoxP and H-2D^b LoxP mice crossed with Cdh5-Cre mice to achieve targeted deletion of discrete class I molecules on brain endothelium. Using the *Plasmodium berghei* ANKA model of experimental cerebral malaria (ECM), we observe that H-2K^b and H-2D^b regulate distinct patterns of disease onset, CD8 T cell infiltration, targeted cell death, and regional blood-brain barrier (BBB) disruption. Strikingly, ablation of H-2K^b or H-2D^b from brain endothelial cells resulted in reduced CD8 T cell activation, attenuated T cell interaction with brain vasculature, lessened targeted cell death, preserved BBB integrity, and prevented ECM and the death of the animal. These data demonstrate that interactions of CD8 T cells with discrete MHC class I molecules on brain endothelium regulate development of ECM neuropathology. Therefore, targeting MHC class I interactions therapeutically may hold potential for treatment of cases of severe malaria.

Introduction

Plasmodium falciparum has been classified as the deadliest parasite by the World Health Organization (WHO). This strain is also the most prevalent malaria parasite, accounting for majority of human infections[1]. Despite initiatives to limit mortality, it is estimated that greater than 600,000 people succumbed to malaria in 2020[2]. A severe complication *of Plasmodium falciparum* is severe encephalopathy, termed cerebral malaria (CM), which results in high mortality despite treatment[3, 4, 5, 6, 7]. CM accounts for approximately 80% of all malaria-related deaths, and patient admissions with CM are steadily increasing annually[2]. The majority of

62 cerebral malaria patients are diagnosed by the presence of asexual parasite in a blood smear,
63 deep coma, and absence of other infectious disease[3, 8]. Other hallmarks of disease can only be
64 assessed post-mortem such as disruption of BBB tight junction proteins, vascular permeability,
65 sequestration of parasitized red blood cell (prbc) and leukocytes, cerebral microhemorrhage and
66 endothelial cell activation[9, 10]. MRI has been gaining traction as a diagnostic tool in patients, as
67 vascular permeability can be assessed via T1 and T2 weighted MRI[10]. Recently,
68 immunohistochemical studies of autopsied human brain specimens have revealed that CD8 T
69 cells have been shown to be tightly associated with brain microvasculature and infiltrate brain
70 parenchyma, implying an important role for this immune cell type in neuropathogenesis[11].
71 *Plasmodium berghei ANKA* (PbA) infection is an established murine model that
72 recapitulates human disease and CNS pathology, referred to as ECM[12]. As in the human disease,
73 CD8 T cell responses are strongly implicated in the neuropathology. Importantly, CD8 T cells
74 are required to have functioning cytotoxic capacity to develop the fatal BBB disruption
75 associated with ECM[13, 14, 15, 16]. An IFN-γ dependent upregulation of adhesion molecules (ICAM-
76 1 and VCAM-1) and molecules associated with antigen (Ag) presentation (MHC Class I
77 molecules D^b and K^b and MHC Class II) has been observed on brain and meningeal endothelial
78 cells day 6 of PbA infection[17]. However, the contribution of specific cell types producing IFN-γ
79 in this pathology have not been interrogated[17]. Interest in these CD8 T cell-endothelial cell
80 interactions, has prompted a concerted effort to define the requirement of Ag-specific CD8 T
81 cells in this neuropathology. Due to the complex life-cycle of the parasite, defined by extensive
82 antigenic variation throughout each stage, this has proven a difficult task. The engagement of
83 CD8 T cells with class I molecules has been functionally assessed with bone marrow chimeras of
84 MHC class I-deficient hosts reconstituted with class I-sufficient hematopoietic presentation[17].

85 However, it is known that CD8 T cells raised in these hosts have inherently impaired
86 development and survival[17, 18]. While this important work narrows in on the significance of non-
87 hematopoietic Ag-presentation in this pathology, the role of Ag-presentation specifically on
88 brain vasculature has not yet been addressed. Furthermore, the contribution of discrete class I
89 molecules in ECM pathology remain undefined.

90 In these studies, we sought to define the contribution of mouse brain microvascular
91 endothelial cell (MBMEC) Ag-presentation by discrete class I molecules to the pathogenesis and
92 lethality of ECM. We hypothesized that conditional ablation of Ag-presentation by H-2K^b and
93 H-2D^b class I molecules on MBMECs would result in controlled modulation of activation and
94 entry of parasite-specific CD8 T cells, attenuating pathology. To test this, we crossed
95 endothelium-specific Cdh5-Cre mice with our novel H-2K^b LoxP and H-2D^b LoxP mice to
96 create cKOs of discrete class I molecules. In these studies, we employed human and mouse
97 transcriptomic data to evaluate gene expression in brains in response to plasmodium expression.
98 We also employed *in vivo* 2-photon imaging to interrogate T cell interactions at the inflamed
99 vasculature of the brain when individual MHC class I molecules are present or conditionally
100 deleted on endothelium during PbA infection. Infiltration, activation, and localization of CD8 T
101 cells and their potential targets were assessed via spectral flow cytometry in these novel
102 transgenic mice. We demonstrate that interactions with specific class I molecules determined
103 CD8 T cell activation, infiltration of the brain and localization and onset of cell death and
104 neuropathology. However, knockout of H-2K^b and H-2D^b in endothelial cells prevented CD8 T
105 cell interactions at brain vasculature, CD8 T cell activation, BBB disruption, cell death and
106 neuropathology. These mice did not develop ECM, resulting in almost complete survival.
107 Together these data demonstrate that CD8 T cells engage H-2K^b or H-2D^b class I molecules on

108 MBMECs in order to coordinate activation, entry, and induction of neuropathology. These
109 studies indicate that modulation of brain microvascular endothelial cell class I restricted Ag-
110 presentation may hold therapeutic benefit in cases of cerebral malaria.
111
112 **Results**
113 **Mouse and human brain microvascular endothelial cells increase antigen presentation**
114 **molecules capable of eliciting T cell responses after *Plasmodium* infection.** C57BL/6 mice
115 were intraperitoneally (I.P.) injected with PbA prbcs, resulting in peripheral infection and
116 manifestation of ECM on days 6-8 (Fig. 1a). Brains were harvested and RNA was extracted from
117 whole brains of infected C57BL/6 mice and uninfected controls (Fig. 1a). Nanostring analysis
118 was performed on bulk RNA for analysis of differential gene expression between uninfected and
119 infected mice (Fig. 1b). Upregulated genes were associated with major immunological pathways,
120 including Ag-presentation, T cell responses, cytotoxicity, cell activation and apoptosis.
121 Downregulated genes were associated with markers of homeostasis or components of blood-
122 brain barrier (Fig. 1b). Gene expression data were analyzed using Ingenuity Pathway Analysis
123 (IPA). Causal network analysis identified MHC Class I family as the most significant master
124 regulator in ECM pathology (Supplementary Table 1). MHC Class I family activation led to
125 downstream activation of the majority of upregulated genes of interest identified in Fig. 1b (Fig.
126 1c). Canonical pathway analysis identified the most differentially enriched signaling pathways
127 during ECM, confirming Ag-presentation as a major pathway of interest (Fig. 1d). MBMECs
128 have been implicated to be involved in Ag-presentation during ECM (Fig. 1e). To interrogate
129 their role, we employed enzymatic digestion and high-dimensional spectral flow cytometry to
130 measure expression of Ag-presentation-associated molecules. MHC Class I median fluorescence

131 intensity is increased on MBMECs during ECM and the percent of expression on MBMECs is
132 significantly higher during ECM (Fig. 1f). MHC Class II is a well-known marker of antigen
133 presenting cells (APCs). MHC Class II expression on MBMECs greatly increased from minimal
134 to high during ECM, implicating their role in Ag-presentation (Fig. 1g). We next interrogated
135 gene expression signatures of human brain microvascular endothelial cells (HBMECs) from
136 human donor after exposure to *Plasmodium falciparum*. To this end, we utilized human
137 microarray dataset from Tripathi et al. (accession GSE9861)[19] in NCBI GEO database. In brief,
138 isolated HBMECs were co-cultured with *Plasmodium falciparum* prbcs or uninfected red blood
139 cells in culture and then analyzed (Fig. 1h). We first assessed the distribution of expression
140 values for each human sample to ensure suitability for comparison (Supplementary Fig. 1a).
141 After human sample validation we evaluated MHC Class I and MHC Class II expression levels.
142 MHC Class I expression was significantly increased in HBMECs exposed to *Plasmodium*
143 *falciparum* infected red blood cells (Fig. 1i). Human samples which were exposed to infection
144 were subdivided into two groups 1) high adhesion molecule expression and 2) low adhesion
145 molecule expression[19] (Supplementary Fig. 1b). MHC Class II expression was shown to be
146 significantly upregulated only in the high adhesion molecule samples compared to controls (Fig.
147 1j). Using GEO2R analysis platform, MHC Class I was identified as one of the most
148 significantly differentially expressed genes and was in the top 5 genes with significant
149 upregulation on HBMECs after exposure to *Plasmodium* infection (Supplementary Table 2).
150 When comparing mouse and human genes involved with Ag-presentation we saw that gene
151 activation and inhibition in these pathways were highly analogous (Supplementary Fig. 2). We
152 also saw comparable upregulation of homologous genes of interest downstream of MHC Class I
153 in human HBMECs, consistent with our observations in the mouse model (Fig. 1k). When

154 performing gene set enrichment analysis (GSEA) on HBMEC transcriptomics data we identified
155 the molecular signature for T cell activation involved in immune response to be highly enriched
156 in HBMECs exposed to infection. The enrichment of this gene set indicates that HBMECs
157 become an APC during *Plasmodium* infection, capable of eliciting this downstream T cell
158 response (Fig. 1l). Together, these results suggest that in both mouse and human, brain
159 endothelial cells are performing Ag-presentation to activate downstream T cell effector activities
160 following *Plasmodium* infection.
161
162 **Endothelial cell specific K^b conditional knockout mice develop normal peripheral**
163 ***Plasmodium* infection and immune responses.** We crossed (class I deficient background, K^b-/-,
164 D^b-/-) K^b LoxP mice with (class I deficient background, K^b-/-, D^b-/-) Cdh5-Cre mice (Fig. 2a).
165 The resulting animals are defined as K^b Cre- littermate (with ubiquitous K^b expression), and
166 Cdh5-Cre K^b cKO (with endothelial-specific ablation of K^b), respectively. At baseline, Cdh5-Cre
167 K^b cKO mice had significantly reduced protein levels of K^b on brain endothelium, as well as
168 reduced percentage of brain endothelial cells that express K^b (Fig. 2b-d). T cell development was
169 intact in Cdh5-Cre K^b cKO and K^b Cre- littermates with no changes in thymic T cell subset
170 frequencies, mTEC and cTEC frequencies, or thymic weights between groups (Fig. 2e-f and
171 Supplementary Fig. 3a). Furthermore, no sex specific differences pertaining to T cell
172 development, overt changes in CD8 T cell repertoire, or change in splenic weights were observed
173 (Supplementary Fig. 3b-d). To determine the effect of K^b class I molecule ablation on MBMECs
174 during ECM, adult Cdh5-Cre K^b cKO (~3-month-old) mice and K^b Cre- littermates were I.P.
175 infected with $1x10^6$ PbA prbcs and tissues were harvested at approximately 6-8 days post
176 infection (dpi) (Fig. 2g). During infection K^b remained significantly reduced on brain

177 endothelium (Fig. 2h-j). In the spleen, we observed no changes to granulocyte or APC subsets
178 during infection in Kb Cre- littermates or Cdh5-Cre K^b cKO mice (Fig. 2k-l). Importantly, there
179 were no differences in the ability to establish blood stage infection in these mice (Fig. 2m).
180 Populations of immune cells were assessed in peripheral tissues at baseline and during infection
181 and showed no changes in CD45+ immune cell numbers between Cre- littermates and Cdh5-Cre
182 K^b cKO spleen, peripheral blood or inguinal LN (Supplementary Fig. 3e). In these peripheral
183 tissues CD4 and CD8 T cell numbers and activation state remained unchanged between groups in
184 all peripheral organs, with the exception of a modest reduction in numbers of activated CD8s at
185 baseline in inguinal LNs in the Cdh5-Cre K^b cKO mice (Supplementary Fig. 3g). However,
186 during PbA infection, there were no differences in CD8 activation in inguinal LNs (Fig. 2o).
187 These results demonstrate that our Cdh5-Cre K^b cKO mouse model has efficient deletion of K^b
188 on vasculature, while maintaining a fully functional peripheral immune response to *Plasmodium*
189 infection. This allows us to proceed with interrogation of potentially brain-specific
190 immunomodulatory functions of K^b Ag-presentation by brain endothelial cells in ECM.
191
192 **Endothelial cell specific D^b conditional knockout mice develop normal peripheral**
193 ***Plasmodium* infection and immune responses.**
194 We crossed (class I deficient background, K^b-/-, D^b-/-) D^b LoxP mice with (class I deficient
195 background, K^b-/-, D^b-/-) Cdh5-Cre mice (Fig. 3a). The resulting animals are defined as either D^b
196 Cre- littermate (with ubiquitous D^b expression), or Cdh5-Cre D^b cKO (with endothelial-specific
197 ablation of D^b). Endothelial cell expression of D^b at baseline in Cdh5-Cre D^b cKO mice was
198 comparable to Cre- littermate controls. Percentage of class I expression on endothelium was
199 reduced but did not reach statistical significance in uninfected Cdh5-Cre D^b cKO mice (Fig. 3b-

200 d). T cell development was intact with no changes in thymic T cell subset frequencies, mTEC
201 and cTEC frequencies, or in thymic weights between groups (Fig. 3e-f and Supplementary Fig.
202 4a). There were no differences between males and females in development of thymic T cell
203 subsets, and no differences between groups in CD8 T cell V beta usage in spleen, or in splenic
204 weights (Supplementary Fig. 4b-d). To determine the effect of D^b class I molecule ablation on
205 MBMECs during ECM, adult Cdh5-Cre D^b cKO (~3-month-old) mice were I.P. infected with
206 PbA and tissues were harvested at onset of severe neurological symptoms, approximately 6-8 dpi
207 (Fig. 3g). Importantly, during infection D^b expression was significantly reduced on brain
208 endothelium (Fig. 3h-j). Spleens of these animals had no changes to granulocyte or APC subsets
209 during infection (Fig. 3k-l) and mice established full blood stage infection in the periphery (Fig.
210 3m). Assessment of immune cell populations in peripheral tissues at baseline and during
211 infection revealed no changes in CD45+ immune cell number between D^b Cre- littermates and
212 Cdh5-Cre D^b cKO in spleen, peripheral blood or inguinal LN (Supplementary Fig. 4e-f). CD4
213 and CD8 T cell numbers and activation state remained unchanged between groups in all
214 peripheral organs at baseline (Supplementary Fig. 4f). However, during infection, there was
215 reduction in number of activated CD8 T cells in inguinal LN in the Cdh5-Cre D^b cKO animals
216 (Fig. 3n-p). These results demonstrate that our Cdh5-Cre D^b cKO mouse model has sufficient
217 deletion of D^b on vasculature during PbA infection and a fully functional peripheral immune
218 response. These results enabled us to proceed with interrogation of potentially brain-specific
219 immunomodulatory functions of D^b Ag-presentation by brain endothelial cells in ECM.
220
221 **T cell dynamics at the barrier are modulated by the presence of distinct class I molecules**
222 **on endothelium.** To assess whether brain vasculature was inherently changed by loss of

223 endothelial class I in cKO mice, we performed maximum intensity projections (MIPs) using MRI
224 angiography to illuminate and assess the blood vessels. Cdh5-Cre K^b cKO and Cdh5-Cre D^b
225 cKO were compared to their respective Cre- littermate controls. At baseline, we observed no
226 differences in 3D volume of overall brain vasculature or voxel units (Supplementary Fig. 5a-b
227 and 5c-d). We therefore proceeded to assess the effects of discrete MHC class I molecules on T
228 cell dynamics in brain vasculature. To address this, we employed acute cranial window
229 placement and *in vivo* two-photon imaging after IV injections of anti-Thy1.2-Alexa Fluor 488 to
230 label T cells in vasculature and Texas Red-Dextran to label vessels. 6-7 days following PbA
231 infection, mice underwent live imaging and T cell interactions at the brain vasculature were
232 tracked over time (Fig. 4a). Cre- Littermates with K^b expression on brain vasculature presented
233 with higher numbers of T cells per field of view (FOV) with slowed velocities, indicating
234 interactions with K^b on endothelium (Fig. 4b and 4c). In contrast, Cdh5-Cre K^b cKO mice, which
235 lack K^b on endothelium, had lower numbers of T cells per FOV, with higher velocity indicating
236 less interactions with endothelium (Fig. 4b and 4c). Interestingly, there were no significant
237 differences between the frequency that T cells contacted the vessels between genotypes.
238 However, arrest on vessels was significantly increased when K^b was expressed on the brain
239 vasculature (Fig. 4d-4e and Supplementary Videos 1-2). To investigate these T cell interactions
240 further, we examined the activation state and adhesion molecule expression of MBMECs. During
241 late-stage PbA infection, endothelial cells upregulate adhesion molecules responsible for
242 initiating T cell extravasation[20]. P-selectin, which facilitates activated T cell rolling, did not
243 differ in expression between Cdh5-Cre K^b cKO mice and Cre- littermates (Fig. 4f). ICAM-1 and
244 VCAM-1 expression, involved in arrest and adhesion, also showed no significant differences
245 during infection (Fig. 4g-h). When endothelial cells are activated, they upregulate molecules

246 involved in Ag-presentation[17]. Surprisingly, when K^b class I molecule expression was ablated,
247 MHC Class II molecules were upregulated on brain endothelium during infection (Fig. 4i).
248 T cell dynamics in Cre- D^b expressing and Cdh5-Cre D^b cKO mice were similar to those
249 of the previous model. 6-7 dpi with PbA T cell interactions with vasculature were tracked over
250 time during intravital imaging (Fig. 4j). Cre- Littermates with D^b present on vasculature showed
251 high numbers of T cells/FOV. In Cdh5-Cre D^b cKO mice, T cells were greatly reduced per FOV,
252 indicating fewer T cells slowed down to interact with endothelium when D^b molecule is ablated
253 on vasculature (Fig. 4k). Meanwhile, D^b expressing Cre- littermate T cells had slower velocities,
254 indicating more interactions with D^b on endothelium. When endothelial D^b is conditionally
255 deleted in Cdh5-Cre D^b cKO mice, T cells that interact with vessels had significantly increased
256 velocities, with reduced slowing and rolling on vasculature (Fig. 4l). Again, there were no
257 significant differences between the percentage of T cells contacting vessel walls between groups.
258 However, the frequency of T cell arrests was significantly increased when D^b was expressed by
259 brain vasculature (Fig. 4m and 4n). (Supplementary Videos 2-3). P-selectin was greatly
260 increased when D^b was present on brain endothelium during infection, indicating a higher
261 probability of activated T cell rolling (Fig. 4o). Interestingly, cells/FOV in the D^b expressing Cre-
262 littermates, had increased cells/FOV compared to K^b Cre- littermates (Fig. 4b and 4k). There
263 were no significant changes in ICAM-1 or VCAM-1 expression on endothelium when D^b was
264 conditionally deleted (Fig. 4p-q). As was seen with K^b cKO mice, deletion of D^b class I molecule
265 on endothelial cells resulted in higher expression of MHC Class II molecules on endothelium in
266 comparison to Cre- littermates (Fig.4i and 4r). Together, this data demonstrates that H-2K^b and
267 H-2D^b class I molecules are critical for optimal T cell adhesion and arrest to brain endothelium
268 during ECM.

269

270 **CD8 T cell activation and infiltration into brain parenchyma is differentially modulated by**
271 **discrete class I molecules during infection.** We next addressed if the changes observed in T
272 cell dynamics at the brain vasculature during PbA infection corresponded with T cell infiltration
273 into brain parenchyma. First, we wanted to confirm that cervical lymph node (cLN) priming of
274 brain draining antigens was intact in our mouse models. To test this, we employed Theiler's
275 murine encephalomyelitis virus (TMEV) and TMEV-OVA. These neurotropic viruses are
276 intracranially administered and provide a highly reproduceable model of CNS antigen drainage
277 resulting in cLN priming, CD8 T cell infiltration, and viral clearance[21, 22, 23]. TMEV
278 immunodominant peptide $VP2_{121-130}$ is presented in the H-$2D^b$ MHC class I molecule whereas
279 TMEV-OVA model antigen $OVA_{257-264}$ is presented by H-$2K^b$ [23]. On day 7 post infection mice
280 were perfused and cLNs were analyzed via spectral flow cytometry (Supplementary Fig. 6a). In
281 mice infected with either TMEV or TMEV-OVA, tetramer staining was unchanged between Cre-
282 and Cre+ mice indicating that cLN priming in these mice is intact (Supplementary Fig. 6b-c). We
283 now evaluated immune cell infiltration into the brain in the ECM model, in which the
284 *Plasmodium* infection arises in the periphery prior to neuroinflammation in the brain (Fig. 5a).
285 At moribund, 6-8 d.p.i., mice were euthanized and perfused. Mouse brains were processed into
286 single cell suspensions and analyzed via spectral flow cytometry. Overall immune populations in
287 the brains during infection can be visualized in the UMAP projection (Fig. 5b). Data
288 encompassing CNS infiltration of immune cells were interrogated. Absolute counts of total
289 CD45+ immune cells in the brain remain unchanged when K^b class I molecules are present on
290 endothelium versus endothelial cell class I molecule conditional knockout mice (Supplementary
291 Fig. 6d). Numbers of CD4 T cells in the brain also remain unchanged regardless of K^b expression

292 by endothelial cells (Fig. 5e). However, when K^b expression is lost on endothelium, CD8 T cell
293 infiltration of the brain is greatly diminished (Fig. 5f). Since adhesion molecule expression on
294 endothelium was previously shown to be unchanged, we also examined CD8 T cells for
295 chemokine receptors involved in trafficking to the CNS and adhesion to the endothelium. Levels
296 of CXCR3, a receptor shown to be necessary for recruitment of T cells into the brain to establish
297 ECM[24, 25], was not impacted by ablation of K^b on vasculature (Supplementary Fig. 6f-g). CCR7,
298 a chemokine receptor known to be upregulated on T cells trafficking to the brain during
299 neuroinflammation, was also evaluated[26]. During ECM the olfactory region highly upregulates
300 CCL21, and blockade of CCR7 decreases T cell activation, recruitment and survival[27]. In Cre-
301 littermates with K^b, we saw no difference in CD8 T cell expression of CCR7 from mice lacking
302 K^b on vasculature (Supplementary Fig. 6h-i). We next evaluated effector status of CD4 and CD8
303 T cells in the brain. Interestingly, CD8 T cells that infiltrated the brain during infection produce
304 significantly less IFN-γ when K^b expression was ablated on vasculature (Fig. 5g). Surprisingly,
305 although brain infiltrating CD4 T cell numbers did not change, these lymphocytes increasingly
306 assumed a Th1 phenotype with increased expression of IFN-γ when K^b was ablated on
307 endothelium (Fig. 5h). In a parallel set of experiments, we investigated whether antigen
308 recognition plays a role in infiltration and localization of IFN-γ producing CD8 T cells. We
309 infected mice and intravenously (IV) injected Alexa Fluor-488 conjugated anti-Thy1.2 antibody
310 3 minutes before euthanasia on day 6 of infection to label cells that have recently infiltrated brain
311 parenchyma from the bloodstream. It is important to note that K^b expressing Cre- mice are not
312 yet moribund on day 6 of infection. We also evaluated surface expression of CD11a as a
313 surrogate marker for cognate antigen-experienced CD8 T cells as previously described [28]. At 6
314 d.p.i. we show that numbers of Ag-experienced CD8 T cells were not different between K^b

315 expressing Cre- and Cdh5-Cre K^b cKO mice in meninges or cervical LNs of PbA infected mice.
316 However, numbers of brain infiltrated Ag-specific CD8 T cells were greatly reduced when K^b
317 was lost on vasculature (Fig.5i). K^b expressing Cre- mice presented with a significant increase of
318 CD11a+ CD8 T cells only in the IV- group, indicating that the majority had infiltrated the brain
319 prior to IV labeling. In Cdh5-Cre K^b cKO mice lacking K^b on vessels, numbers of both IV- and
320 IV+ CD8 T cells were greatly reduced, demonstrating that recognition of peptides presented by
321 K^b is required for optimal CD8 T cell infiltration (Fig. 5j). It is known that IFN-γ producing CD8
322 T cells have enhanced Ag-specific contacts, cytolytic killing and kinetics through paracrine and
323 autocrine IFN-γ signaling[29]. We therefore employed IV labeling to determine the localization of
324 IFN-γ producing CD8 T cells 6 d.p.i with PbA. We noted a slight trend towards increased
325 frequency of IFN-γ producing CD8 T cells in the recently infiltrated IV+ population in both Cre-
326 and Cre+ animals. However, this difference did not reach significance (Fig5k).
327 We next assessed the immune profile of the brains of D^b expressing mice in ECM.
328 Tissues were harvested at moribund, days 6-8 of infection. We observed no difference in the
329 overall numbers of CD45+ immune cells in the brain between D^b expressing Cre- and Cdh5-Cre
330 D^b cKO mice (Supplementary Fig. 6e). Surprisingly, we observed no change in CD8 T cell
331 infiltration between the groups, and numbers of CD4 T cells in the brain were also unchanged
332 (Fig. 5l-o). Expression of trafficking and adhesion molecules on CD8 T cells were assessed and
333 levels of CXCR3 and CCR7 were not significantly different between D^b Cre- littermates and
334 Cdh5-Cre D^b cKO (Supplementary Fig. 6j-m). Although overall brain infiltration of CD8 T cells
335 was unchanged, these lymphocytes presented with reduced IFN-γ production when D^b was
336 ablated on vasculature (Fig. 5p). In contrast, no change in CD4 T cell IFN-γ production was
337 observed (Fig. 5q). When assessing the role of Ag-recognition in infiltration, we observed 6

338 d.p.i. that numbers of CD11a+ Ag-experienced CD8 T cells were not different between Cre- and
339 Cdh5-Cre D^b cKO mice in meninges or cervical LNs. However, numbers of brain infiltrating
340 CD11a+ Ag-experienced CD8 T cells were significantly reduced when D^b was lost on
341 vasculature (Fig. 5r). We observed that numbers of previously infiltrated, IV- Ag-experienced
342 CD8 T cells were much lower in D^b Cre- mice than in K^b Cre- mice, although the IV+
343 populations between Cre-s were more comparable on day 6 of infection (Fig. 5j and 5s). This
344 suggests that Ag-specific CD8 T cell infiltration may begin at a later timepoint and escalate more
345 quickly with D^b on endothelium in comparison to K^b. Alternatively, we may not see a difference
346 between IV- and IV+ if vascular leakage is present as this could result in increased antibody
347 staining in the parenchyma (Fig. 5s). The previously infiltrated, Ag-experienced CD8 T cells in
348 the D^b Cre- littermates were significantly increased only when compared to the IV+ population
349 in the D^b cKO mice (Fig. 5s).

350 It is important to highlight that total numbers of brain infiltrated CD8 T cells are similar
351 between Cre- littermates (with either K^b or D^b) at endpoint (Fig. 5f and 5o). However, Ag-
352 experienced CD11a+ CD8 T cell numbers were much higher in K^b expressing than in D^b
353 expressing Cre- controls (Fig. 5i and 5r). As per localization of IFN-γ producing CD8 T cells, D^b
354 expressing Cre- animals had significantly increased frequency of CD8 T cells producing IFN-γ
355 in the IV labeled population on day 6 of infection, suggesting these cells have increased effector
356 function when recently infiltrated from vasculature (Fig. 5t). Meanwhile, Cdh5-Cre D^b cKO
357 animals had no change in frequency of IFN-γ producing CD8 T cells between IV+ and IV-
358 groups (Fig. 5t).

359 To further interrogate infiltration, we compared rates of entry of Ag-experienced
360 (CD11a+) and Ag-inexperienced (CD11a-) CD8 T cells on day 6 of infection. We observed that

361 CD11a+ Ag-experienced CD8 T cells in mice with K^b or D^b expression had faster infiltration
362 than mice with conditional deletion of class I molecules on endothelial cells, though this did not
363 reach significance in D^b cKO mice (Supplementary Fig. 6n-o). CD8 T cells that were CD11a-
364 (Ag-inexperienced) in K^b expressing mice had low rates of infiltration and there was not a
365 significance difference in infiltration between K^b Cre- and Cdh5-Cre K^b cKO mice
366 (Supplementary Fig. 6p). These data suggest that K^b class I molecule is important for Ag-specific
367 CD8 T cell brain infiltration in ECM. Although no differences were seen in CD11a- Ag-
368 inexperienced CD8 T cell rates of entry in between Cre- and D^b cKO mice, D^b expressing Cre-
369 mice rate of CD11a- CD8 T cell entry was double that of K^b expressing Cre- animals
370 (Supplementary Fig. 6p and q). Importantly, the same number of activated IFN-y producing CD8
371 T cells end up in the brain of K^b and D^b Cre- littermates at endpoint despite numbers of CD11a+
372 Ag-experienced CD8 T cells in D^b expressing mice being much lower on day 6 (Fig. 5g and p).
373 This demonstrates that D^b class I molecule on endothelium is required to initiate IFN-y
374 production by CD8 T cells to the same extent as K^b, and that each class I molecule on
375 endothelium differentially modulates the timeline of entry of Ag-specific CD8 T cells.
376 It is known that most neuropathology and vascular leakage during CM and ECM localize
377 to three distinct regions of the brain; olfactory, hippocampus and brainstem[16]. We therefore
378 wanted to assess whether infiltrating CD8 T cells enter brain parenchyma in these regions. Using
379 2-photon and confocal microscopy, we imaged cell dynamics and performed
380 immunofluorescence staining on brain tissues at late stages of infection. At 6-7 dpi we observed
381 CD8 T cells extravasating via post-capillary venules and entering regions of brain parenchyma in
382 K^b expressing Cre- mice (Supplementary Video 5). In K^b expressing Cre- littermates, we
383 observed parenchymal CD8 T cells in olfactory, brainstem, and hippocampal regions. However,

384 when K^b is deleted on vasculature, CD8 T cell infiltration into these regions is greatly decreased
385 (Supplementary Fig. 6r). When imaging D^b expressing Cre- littermates, we saw CD8 T cell
386 infiltration into brain parenchyma (Supplementary Video 6). We also confirmed that when D^b
387 expression is ablated on vasculature, CD8 T cells are still present in brain parenchyma in these
388 three regions (Supplementary Fig. 6s). These data support the findings of our spectral flow
389 cytometry data and demonstrate that CD8 T cells are infiltrated into regions of the brain affected
390 by ECM, except specifically when K^b is deleted on brain vasculature.
391
392 **Blood-brain barrier disruption is dependent on MHC Class I molecule expression by brain**
393 **endothelium.** Next, we assessed the contribution of discrete class I molecules on modulating
394 BBB disruption during ECM. At 6-8 dpi with PbA, mice were administered gadolinium I.P. and
395 evaluated for vascular permeability in the brain using T1-weighted gadolinium enhanced MRI.
396 In Cre- mice with K^b class I molecule expression intact, we see significant enhancement in
397 regions of olfactory bulb, brainstem and hippocampal regions periventricular to the lateral
398 ventricles (Fig 6a). All areas of leakage were assessed utilizing 3D volumetric analysis with
399 Analyze Software as previously described[16]. Brain vascular integrity was retained, and
400 gadolinium leakage was not observed when K^b expression was ablated on vasculature (Fig. 6a-
401 c). As a secondary method of vascular leakage assessment, we IV injected ~66 kDa FITC-
402 albumin, one hour prior to tissue harvest. FITC-albumin mean fluorescence intensity was
403 quantified in our three brain regions of interest. Uninfected and infected wildtype C57BL/6 mice
404 were included as visual reference controls (Fig. 6d). Cre- littermates with K^b expression had
405 significant FITC-albumin leakage in regions of olfactory bulb and brainstem. In contrast, Cdh5-
406 Cre K^b cKO animals lacking K^b on vasculature had negligible BBB disruption, indistinguishable

407 from uninfected controls (Fig. 6d). FITC-albumin leakage is quantified in Fig. 6e. PbA infected
408 D^b expressing Cre- Littermates presented with even more pronounced gadolinium-enhancement
409 in regions of interest than K^b expressing Cre- mice as measured by small animal MRI (Fig. 6a-c
410 and 6f-h). Cdh5-Cre D^b cKO mice however, presented with an intact blood brain barrier, with no
411 notable pathology when D^b is lost on vasculature during infection (Fig. 6f-h). In a secondary
412 analysis utilizing FITC-albumin leakage, we observed increased FITC-albumin mean
413 fluorescence intensity in D^b expressing Cre- olfactory bulb and brainstem (Fig. 6i-j). In Cdh5-
414 Cre D^b cKO mice, brain vascular integrity was retained, and no FITC-albumin leakage was
415 observed (Fig. 6i-j). Tight junction proteins are known to be downregulated in regions of BBB
416 disruption[16]. In human endothelial cells exposed to *Plasmodium falciparum* prbcs *ex vivo*, we
417 observed negative enrichment scores consistent with downregulation of tight junction proteins
418 (Supplementary Fig. 7a). We next performed Claudin-5 staining in our K^b and D^b models,
419 interrogating the regions of vascular leakage in the brains, where T cells were also observed to
420 infiltrate (Supplementary Fig. 8r-s). We saw that the vessels in regions of leakage and CD8 T
421 cell infiltration in both K^b and D^b Cre- littermates had a more sparse and punctate staining for
422 Claudin-5, indicating tight junction protein alteration (Supplementary Fig. 7b-c). However, K^b
423 and D^b cKO animals lacking class I molecules on vasculature had intact Claudin-5 expression
424 along vessels, despite the CD8 T cell infiltration seen in the Cdh5-Cre D^b cKO mice
425 (Supplementary Fig. 7b-c). Overall, these results indicate that vascular leakage and disruption of
426 BBB tight junctions occurs in mice via class I molecule restricted antigen presentation by brain
427 endothelium during *Plasmodium* infection.
428

429 **PbA infected parabionts sharing peripheral circulation demonstrate critical importance of**
430 **endothelial D^b expression to onset of ECM.** Previously, we had noted a decreased number of
431 activated CD8 T cells in inguinal LNs of PbA infected Cdh5-Cre D^b cKO mice (Fig. 3p). In
432 order to further rule out peripheral immune perturbations and fully demonstrate that
433 neuropathology was dependent on CD8 T cell interactions with MBMECs, we performed
434 parabiosis (Fig. 7a). Surgery was performed to conjoin D^b expressing Cre- littermate controls
435 with Cdh5-Cre D^b cKO mice in order to exchange peripheral blood and circulating immune cells.
436 Three weeks of healing and acclimation were observed before both mice were I.P. injected with
437 PbA to induce ECM (Fig. 7b). Our analysis revealed that all peripheral immune activation was
438 similar in the spleen and inguinal LNs of parabionts after infection (Fig.7c-d). In the brain, no
439 differences in CD45+ immune cell frequencies were observed and CD8 and CD4 T cell numbers
440 mirrored that of the previous mouse cohorts with no difference between groups (Fig. 7e). Also
441 consistent with prior cohorts, the Cdh5-Cre D^b cKO parabionts had decreased IFN-γ expression
442 by brain infiltrating CD8 T cells (Fig. 7e). We performed vascular permeability assays in our D^b
443 expressing Cre- to Cdh5-Cre D^b cKO parabionts and determined that the vascular leakage
444 phenotype was consistent with our previous data on D^b Cre- mice and had enhanced FITC-
445 albumin leakage. In contrast, despite having circulating immune cells from D^b expressing Cre-
446 mice, Cdh5-Cre D^b cKO mice resembled uninfected mice in that no vascular permeability was
447 detectable, directly supporting our previous data (Fig. 7f). This observation was further
448 supported by our results employing dual gadolinium enhanced T1-weighted MRI on the
449 parabionts. We observed diffuse enhancement throughout the brain of the Cre- parabiont,
450 indicating leakage. However, the conjoined Cdh5-Cre D^b cKO mice presented with no vascular
451 leakage as demonstrated by lack of gadolinium-enhancement with T1-weighted MRI and

452 retainment of FITC-albumin within vasculature (Fig. 7g). This data confirms that peripheral
453 immunity was not impeded and that changes in infiltration and activation status are truly barrier
454 and brain-specific and are impacted by class I restricted antigen presentation by MBMECs.
455
456 **Differential Endothelial Class I expression alters the neuroinflammatory profile of the**
457 **brain and targeted cell death during ECM.** To define downstream genes discretely regulated
458 by either K^b class I molecule or D^b class I molecule, we examined RNA transcriptomics data for
459 differentially regulated genes in PbA infected wildtype C57BL/6, K^b Cre-, Cdh5-Cre K^b cKO, D^b
460 Cre-, Cdh5-Cre D^b cKO, and uninfected controls of each group. We observed overlaps in gene
461 expression that were shared between wildtype C57BL/6 mice (with K^b and D^b) and K^b Cre- mice
462 (K^b only) (Fig. 8a). Gene programs regulated by K^b were genes primarily expressed in anti-
463 inflammatory A2 astrocytes, primed microglia, and cytokine and interferon signaling (Fig 8a and
464 Supplementary Table 3). Cdh5-Cre K^b cKO mice had very few differentially regulated genes,
465 similar to uninfected mice (Supplementary Figure 8a-c). We also noted distinctively differential
466 expression of genes that overlap between wildtype (with K^b and D^b) and D^b Cre- mice (D^b only)
467 (Fig. 8a). Gene programs regulated by D^b Cre- mice were indicative of a pro-inflammatory A1
468 astrocytic response, stage 2 damage-associated microglia, and microglial neurodegenerative
469 phenotype signatures[30, 31, 32, 33] .We also noted upregulation of genes associated with enhanced
470 Ag-presentation and cytotoxic T cell responses in the brains of these animals, indicating a strong
471 T cell response in these animals (Fig. 8a and Supplementary Table 3). Cdh5-Cre D^b cKO mice
472 had very few differentially regulated genes (Supplementary Figure 8d-f). Overall, the differential
473 gene expression observed between mice expressing distinct class I molecules further supports the
474 independent roles each class I contributes to this pathology.

475 We next wanted to determine what cells are being targeted by infiltrating CD8 T cells
476 during PbA infection. We infected mice with PbA and harvested tissue early on day 6 before all
477 mice were moribund. Brains were harvested to stain with a panel of antibodies to detect stages of
478 cell death. In K^b expressing Cre- littermates, we observed no significant increases in cell death of
479 MBMECs on day 6 of infection and no differences when K^b is deleted on vasculature (Fig. 8b).
480 When assessing neuronal cell death however, there were increased frequencies of cells with early
481 apoptotic markers, but complete neuronal cell death was not detectable by flow at this time.
482 There were no differences between K^b expressing Cre- littermates and Cdh5-Cre K^b cKO mice
483 (Fig. 8c). The low levels of endothelial and neuronal cell death may be attributed to the fact that
484 pathology is delayed in K^b mice in comparison to D^b mice. The K^b Cre- mice have average
485 clinical scores of ~1.5 on day 6 for ECM neurological signs, whereas D^b Cre- mice have average
486 clinical scores of >3 day on 6 (Fig. 8d and 8h). This delay in pathology may also translate to a
487 delay of neuronal and/or endothelial cell targeting as well. To examine this, we performed
488 another experiment in which all mice were allowed to progress to humane endpoint.
489 Transcriptomics analysis revealed that neurons do activate cell death pathways at this late
490 timepoint in K^b Cre- littermates (Fig. 8j). No endothelial cell death pathway activation was
491 noted. Cdh5-Cre K^b cKO mice had significantly improved clinical scores when K^b on
492 vasculature was deleted (Fig. 8d). In extended survival studies, we observed nearly complete
493 survival of Cdh5-Cre K^b cKO mice in comparison to Cre- littermate controls (Fig. 8e).
494 When assessing D^b mouse cohorts at day 6, we observed a striking increase in MBMEC
495 cell death in Cre- littermates that have D^b in comparison to Cdh5-Cre D^b cKO mice (Fig. 8f). A
496 significant increase in neuronal cell death was observed in D^b expressing Cre- littermates in
497 comparison to Cdh5-Cre D^b cKO mice (Fig. 8g). Similar to our observations in K^b, we observed

498 increased frequency of neurons with early apoptotic markers in the Cdh5-Cre D^b cKO mice, but
499 not late-stage neuronal death (Fig. 8g). These data were in agreement with transcriptomics data
500 showing activation of cell death pathways only in D^b Cre- mice (Fig. 8j). In an extended survival
501 study, mice with deletion of D^b on vasculature presented with striking improvement in clinical
502 scores and overall survival (Fig. 8h-i). Overall, neuronal cell death related gene expression was
503 increased in infected wildtype C57BL/6, K^b expressing Cre- mice and D^b expressing Cre- mice
504 (Fig. 8j). These studies demonstrate that class I molecule expression by endothelium is required
505 for the onset of neuronal cell death in the ECM model and that MBMECs undergo cell death late
506 in pathology following D^b MHC Class I-specific-CD8 interactions at vasculature.
507

508 **Discussion**

509 The role of Ag-presentation by brain endothelium and the effect on the CD8 T cell
510 effector response as a putative mechanism of CM have been highly debated in the cerebral
511 malaria field[3, 25, 34]. However, the role of individual class I molecule presentation by MBMECs to
512 brain infiltrating CD8 T cells has never been directly tested *in vivo*. In this study, we demonstrate
513 that targeted deletion of either K^b or D^b class I molecule on endothelium results in reduced T cell
514 interactions at brain vasculature and subsequently attenuated BBB disruption and
515 neuropathology. Comparisons to human data supports these findings, as well as other recent
516 studies which highlighted the importance of CD8 T cell interactions at the vasculature in the
517 development of CM and ECM[11, 17]. Overall, peripheral infection and all immune responses
518 develop normally in our mice, with the exception of mild decrease in CD8 T cell activation
519 marker CD44 at baseline in non-brain draining inguinal lymph nodes in Cdh5-Cre K^b cKO mice.
520 However, this difference resolves during infection. In Cdh5-Cre D^b cKO animals there was also

521 a slight decrease in the CD8 T cell activation marker CD44 in non-brain draining inguinal lymph
522 nodes during PbA infection. We addressed the potential effects these differences could pose in
523 ECM by performing parabiosis, which efficiently equalizes peripheral immune responses.
524 Endothelial cell-specific deletion of class I molecule was still protective, effectively ruling out
525 potential peripheral immune perturbations as having a role in protection from ECM.

526 CD8 T cells have been observed to interact with brain vasculature during
527 neuroinflammation[17, 26, 35, 36, 37]. However, few of these molecular interactions have been
528 successfully interrogated. The most well-characterized of these interactions is the CD8 T cell
529 slowing, rolling, and arrest on brain endothelium[38, 39, 40, 41, 42]. Using intravital microscopy on live
530 mice 6-7 dpi with PbA, we observe high numbers of T cells in both K^b and D^b expressing Cre-
531 littermates exhibiting slowing, rolling and arresting. In contrast, we observed a drop in these T
532 cell interactions with brain vasculature with the loss of either K^b or D^b class I expression by
533 endothelial cells. The novelty of these findings, however, lies in the fact that the adhesion
534 molecule expression is completely unchanged between Cre- and Cre+ animals in the K^b model.
535 This implies that the complete loss of T cell interactions we visualize by 2-photon are dependent
536 on the T cell-K^b class I interaction and not adhesion molecules. In D^b expressing Cre- mice, we
537 observe upregulation of P-selectin on brain endothelium. Surprisingly, despite their essential role
538 in T-cell rolling in vasculature, absence of E or P-selectin in mice have been experimentally
539 shown to be unnecessary for T-cell entry into the CNS, suggesting that T cell rolling is not
540 required for T-cell migration across inflamed BBB [39, 40, 41, 42]. However, most studies focusing on
541 diapedesis interrogated CD4 T cell interactions. ICAM-1 and VCAM-1 on endothelium was not
542 altered when class I molecules were ablated on vascular endothelial cells. Interestingly, when
543 either class I molecule was deleted on endothelium, expression of MHC Class II molecules was

544 found to be elevated. This may be a compensatory mechanism employed by endothelial cells in
545 order to establish a more robust CD4 T cell response when the CD8 T cell response is
546 impaired[43]. The ability of brain endothelium to shift the T cell effector response in the brain is in
547 agreement with several studies which propose that endothelial cell Ag-presentation may have
548 important immunomodulatory functions[35, 36, 37, 44].

549 Observing that deletion of both K^b and D^b class I molecule on endothelial cells resulted in
550 loss of T cell interactions with brain vasculature, we expected this may result in loss of CD8 T
551 cell infiltration. Interestingly, we observed differential CD8 T cell infiltration into brain
552 parenchyma. In Cdh5-Cre K^b cKO mice, we saw a reduction of CD8 T cells infiltrating the brain.
553 However, in Cdh5-Cre D^b cKO mice, we saw no changes in CD8 T cell infiltration, indicating
554 that overall CD8 T cell infiltration and D^b-restriction may be uncoupled in this model. Although
555 the deletion of D^b does not seem to affect overall infiltration of CD8 T cells, lack of D^b does alter
556 effector status. It is known that PbA strain of *Plasmodium* causes brain specific sequestration of
557 prbcs and activation of brain microvasculature[25]. However, work describing the PbA antigenic
558 D^b-restricted peptide SQLLNAKYL showed that when mice are infected with strains of
559 *Plasmodium* that do not cause adherence of prbcs to brain endothelium, CD8 T cells still entered
560 the brain but were not activated, resulting in absence of neurological symptoms in these
561 animals[45]. This supports our findings that when *Plasmodium* initiates endothelial cell Ag-
562 presentation, D^b is required for activation of CD8 T cells, but not infiltration during infection.
563 Furthermore, CD8 T cell TCR binding to cognate peptide presented by both H-2K^b and H-2D^b
564 on brain endothelium resulted in IFN-γ production by infiltrating CD8 T cells, which in turn,
565 caused differentially regulated cell death and mortality of the animal. This is supported by other
566 works showing that IFN-γ production induces a cascade to recruit more CD8 T cells to the

567 brain[43, 45, 46]. Overall, we demonstrated that endothelial K^b class I molecule interactions with
568 CD8 T cells is important for infiltration and activation, while endothelial D^b class I molecule
569 interactions activate CD8 T cells but does not influence diapedesis into parenchyma.

570 Previous work from our lab and others has hinted at the importance of antigen-specificity
571 of these infiltrating CD8 T cells in ECM neuropathology[16, 25, 45, 47]. However, definitive support
572 for this has been elusive and incomplete[17, 45 48]. Studies with transgenic parasites bearing model
573 epitopes are unable to recapitulate the complexity of the diverse CD8 T cell responses against the
574 wide array of native malaria Ags seen in mice and humans[49]. The epitopes that are known have
575 been shown to elicit variable CD8 T cell responses[49]. Although epitope discovery continues to
576 be an active area of research, there are currently only 83 known T cell epitopes for PbA out of
577 what is projected to be many thousands[35, 45, 50]. Importantly, a role for BBB damage-associated
578 molecular patterns (DAMPs) or parenchymal brain draining DAMPs in eliciting CD8 T cell
579 responses, have also not been ruled out[25, 34, 49, 50]. To date, our novel mouse models are the first
580 models capable of distinguishing between K^b and D^b class I restricted Ags specifically presented
581 by brain endothelial cells for interrogation of ECM pathogenesis. To assess the role of cognate
582 TCR-MHC interactions in CD8 T cell infiltration in this pathology, we used the well-established
583 surrogate marker strategy to track Ag-experienced CD8 T cells[28]. We saw no differences in Ag-
584 experienced CD8 T cells in the meninges or cervical LNs in either model. However, Ag-
585 experienced CD11a+ CD8 T cells were reduced specifically in brain parenchyma when lacking
586 K^b or D^b on vasculature[28, 51]. We also employed IV labeling of these infiltrating Ag-experienced
587 CD8 T cells 3 minutes prior to harvesting tissue. The caveat of this work is that IV labeling may
588 increase in parenchyma with increased vascular permeability, although this does not seem to be
589 the case in the K^b model. We saw that infiltration is much higher in K^b Cre- littermates than in

590 Cdh5-Cre K^b cKO mice at day 6, and that most CD8 T cells had previously infiltrated over time
591 prior to IV administration of labeling antibody. In the D^b model, however, we see comparable
592 amounts of IV labeled and IV negative cells in the brain indicating that a large influx of CD8 T
593 cells begins day 6 of pathology. These data suggest that K^b Ag-presentation by brain
594 endothelium tightly regulates activation and entry. However, D^b Ag-presentation by brain
595 endothelium does not employ as strict of regulation of CD8 T cell infiltration at the barrier. This
596 may mean that another predominant interaction, by a currently undefined cell type or chemokine
597 gradient, may be initiating this brain infiltration. This other interaction, however, does not
598 sufficiently activate the T cell as is seen when brain endothelium presents on D^b. Overall, these
599 data suggest that CD8 T cell activation and infiltration are influenced differentially in the D^b
600 model during ECM.

601 The chemokine receptor expression of activated T cells shows dynamic plasticity.
602 Several factors, including strength of antigenic signals, tissue-specific imprinting by priming
603 DCs, or cytokine milieu can influence the trafficking of T cells[52]. Both CXCR3 and CCR7 are
604 receptors on CD8 T cells shown to be necessary for recruitment into the brain to establish
605 ECM[24, 25, 26]. During ECM, olfactory bulb and brainstem are physically and functionally
606 damaged, with high prbc and leukocyte sequestration in these regions, which coincides with
607 vascular pathology and neuronal cell death[17, 27]. Specifically, the olfactory region has been
608 shown to highly upregulate CCL21, while brain endothelial cells highly express CXCL9 and
609 neurons highly express CXCL10[24, 27, 53]. Blocking their receptors CCR7 and CXCR3 results in
610 decreased CD8 T cell activation and recruitment to the CNS, respectively, as well as prolonging
611 survival during ECM[27, 54]. To support that T cells were sufficiently primed in the periphery and
612 imprinted for CNS-specific trafficking we examined chemokine receptor expression on CD8 T

613 cells trafficking to the brain. In the brain, frequency of CD8 T cells expressing CXCR3 and
614 CCR7, and MFIs of receptor expression were unchanged between Cre- and cKO animals in both
615 models; thereby reinforcing brain-specificity. The majority of data on CD8 T cell infiltration in
616 ECM focuses on the cortex, as this is the brain region most heavily infiltrated by CD8 T cells
617 during this pathology[55]. However, no prior reports have shown regional infiltration of areas
618 affected by vascular permeability. In this work we not only show regional CD8 infiltration to
619 areas with highest brain pathology, but that CD8 T cells are also present in regions without
620 vascular leakage, a topic previously debated[17].

621 CNS vascular leakage was prevalent in both K^b and D^b class I molecule expressing mice.
622 However, the presentation was distinct. In comparison to wildtype C57BL/6 animals, in which
623 both class I molecules are expressed, we saw less leakage in the midbrain of K^b expressing
624 animals, although there was still significant damage and leakage to olfactory and brainstem
625 regions. Alternatively, D^b expressing animals presented with worsened pathology, more closely
626 resembling that of the wildtype C57BL/6 mice which express both class I molecules.
627 Importantly, when either K^b or D^b were ablated specifically from vasculature, there was
628 complete rescue of vascular permeability. This finding is highly novel and strongly suggests that
629 antigens are being presented by either K^b or D^b class I molecules, specifically by brain
630 endothelial cells, to elicit distinct neuropathology associated with ECM. We also show that
631 Claudin-5 is altered in regions of permeability in Cre- animals, a known hallmark of vascular
632 pathology in this disease[16, 17]. However, animals lacking class I on vasculature preserved normal
633 Claudin-5 expression in the regions of interest.

634 We observed that K^b and D^b Ag-specific activation of recently infiltrated CD8 T cells
635 expressing IFN-γ correlates with differential vascular permeability in ECM. We therefore wanted

636 to interrogate whether K^b and D^b class I molecules produced differential activation of
637 neuroinflammatory pathways. We did observe distinct patterns of neuroinflammation, with
638 differential activation of astrocytes and changes in microglial and T cell activation states. This
639 may explain why D^b restricted Ag-presentation on endothelium, though resulting in later
640 infiltration of Ag-experienced CD8 T cells than K^b restriction on day 6, still resulted in stronger
641 T cell signaling, more cell death and worsened vascular leakage and survival at endpoint. Taken
642 together, these data indicate that discrete class I molecules on brain endothelium have
643 immunomodulatory capacity, capable of altering the neuroinflammatory profile of the brain
644 during ECM.

645 Knowing that K^b-restriction and D^b-restriction incite differential neuroinflammatory
646 profiles in the brain during PbA infection, we next sought to determine whether cellular targets
647 of the CD8 T cells were also distinct. We demonstrated that 6 dpi, mice with K^b class I
648 molecules displayed no markers of apoptosis or cell death in vascular endothelium. However,
649 neurons had early apoptotic markers and transcriptomic data supported that neuronal death is
650 induced at endpoint. When K^b was deleted from vasculature, endothelial cells were unchanged.
651 However, neurons no longer acquired the gene signature indicative of neuronal death. This data
652 suggests that CD8 T cell interactions with K^b-restricted Ag-presenting endothelial cells are not
653 required for targeted killing of MBMECs but are supportive of apoptotic neuronal cell death late
654 in pathology. The K^b-CD8 T cell interaction has been shown to modulate infiltration and
655 activation of CD8 T cells and may be involved in CNS reactivation or serve an imprinting role
656 which may instruct CD8 T cells to exact their effector functions in other ways or on other cell
657 types. When assessing D^b Cre- littermates, we observed a large percentage of cell death of
658 MBMECs which was ameliorated when D^b was deleted on vasculature. There was also an

659 increased percentage of cell death seen in neurons in D^b expressing Cre- animals which was
660 either resolved or delayed when D^b was lost on vasculature. This data demonstrates a
661 requirement for D^b-restricted Ag-presentation to CD8 T cells by the vasculature in order to enact
662 an effector response resulting in killing of both MBMECs and ultimately neuronal cell death.
663 The extent to which neuronal cell death is the result of direct killing by CD8 T cells, or through
664 alternative mechanisms has yet to be explored in these models. In previous work which detailed
665 CD8 T cell responses during ECM, they demonstrated that K^b and D^b are capable of presenting
666 similar peptides, though with very different binding affinities[49]. It is also known that receptor
667 affinities control effector responses and T cell polyfunctionality[45, 56, 57, 58, 59]. This is consistent
668 with our data showing that endothelial cells die when D^b presents, but not when K^b presents,
669 dependent upon the differential peptides they display as well as the strength of their interactions.
670 These results prove to be highly innovative as this is the first time that *in vivo* evidence has
671 directly shown the effects of K^b or D^b restricted Ag-presentation by brain endothelial cells during
672 ECM. Follow-up investigations should address direct mechanisms of cell death in more detail.
673 Alterations of cytokine milieu, the impact of vascular leakage and blood-derived factors on
674 neuroinflammation and CD8 T cell responsiveness still must be addressed.
675 In conclusion, our studies provide the first *in vivo* interrogation of the role of Ag-
676 presentation by individual class I molecules by MBMECs in developing ECM pathology. We
677 have dissected the contribution of both K^b and D^b to the onset of neuropathology and provide
678 evidence to support that K^b-restricted Ag engagement on endothelium plays a critical role in
679 CD8 T cell vascular adhesion, arrest, infiltration, and activation. These events in turn contribute
680 to blood-brain barrier tight junction downregulation, vascular leakage, and neuronal death.
681 Meanwhile, D^b-restricted Ag engagement on endothelium plays a role in vascular adhesion and

682 arrest but is inconsequential for CD8 T cell infiltration into brain parenchyma. However, the
683 interaction is important for CD8 T cell activation and IFN-γ secretion which is associated with
684 heightened CD8 T cell motility and toxicity, tight junction downregulation, and vascular
685 permeability[25, 29, 46, 60]. Strikingly, we show that only CD8 TCR recognition of D^b-restricted
686 antigens by brain vasculature results in killing of MBMECs and subsequent neuronal cell death.
687 We contend that these insights into the pathogenesis of cerebral malaria will provide rationale for
688 therapeutic targeting of these interactions. Anti-malarial drugs can serve to lessen parasite
689 burden, but show no improvement in neurological symptoms once there is brain involvement[17].
690 We therefore propose that patients with CM may benefit from endothelial-specific therapeutics
691 which serve to specifically blockade T cell-class I interaction in addition to standard-of-care anti-
692 malarial drugs.
693

694 **Methods**

695 **Animals.** Male and female C57BL/6J WT (stock no. 000664) and Cdh5-Cre mice (stock no.
696 033055) were purchased from Jackson Laboratory. H-$2K^b$ LoxP and H-$2D^b$ LoxP mice were
697 generated by our program as previously described, in the C57BL/6 background [61, 62]. H-$2K^b$
698 LoxP and H-$2D^b$ LoxP mice were crossed with Cdh5-Cre mice to generate Cdh5-Cre K^b cKO
699 and Cdh5-Cre D^b cKO mice that express Cre under the *Cdh5* promoter and undergo endothelial-
700 specific targeted gene deletion of H-$2K^b$ and H-$2D^b$ molecules. Mice were then bred and
701 maintained under specific pathogen free conditions at the Mayo Clinic Animal Facility. In the
702 studies, 15–20-week-old mice were used for all experiments with appropriate age and sex-
703 matched controls. All experiments were conducted in accordance with guidelines from the

704 National Institutes of Health and under the approval of the Mayo Clinic Institutional Animal
705 Care and Use Committee.
706
707 ***Plasmodium* infection.** *Plasmodium berghei* ANKA (PbA) stocks were generously provided by
708 J. Harty at the University of Iowa and S. Hamilton Hart at the University of Minnesota Medical
709 School. PbA infection was induced in 15–20-week-old mice via intraperitoneal injection of ~10^6
710 parasitized red blood cells on day 0. Mice were monitored twice daily until onset of clinical signs
711 were observed (days 6-8 post infection), and then continuously. Blinded scores were obtained
712 daily, scoring signs of neurological impairment until endpoint. Mice were ranked for clinical
713 signs of ECM adapted from Hortle et al[63]: 0, no clinical symptoms; 1, reduced movement and
714 limp/flaccid tail; 2, rapid breathing and transient hunching posture; 3, hunched, ruffled fur and
715 loss strength in four limb hang test; 4, severe disease (ataxia, seizures, coma); and 5, death.
716 Moribund animals were scored 4.5 and humanely euthanized. Mice were classified as having
717 ECM if displaying symptoms between days 6-8 post-infection. Peripheral parasitemia was
718 assessed using thin blood smears and Geimsa staining as outlined on the Centers for Disease
719 Control website and as previously described[64].
720
721 **Acute TMEV and TMEV-OVA Infection**
722 The Daniel's strain of TMEV was prepared as previously described[62]. TMEV-XhoI-OVA8
723 (TMEV-OVA) was generated and prepared by our group as previously described[23]. At 10-12
724 weeks of age, mice were anesthetized with 1-2% isoflurane and infected intracranially (i.c.) with
725 2 x 10^6 PFU (10μL) of the Daniel's strain of TMEV, or 2 x 10^5 PFU of TMEV-OVA. Virus was
726 delivered to the right hemisphere of the brain via automatic 1 mL Hamilton syringe (Hamilton

727 Company, Reno, NV). Mice were euthanized for high-dimensional flow cytometry of tissues at
728 7-days post infection (dpi).
729
730 **Magnetic resonance imaging (MRI).** MRI capture and analysis was conducted as previously
731 reported using Bruker Avance II 7 Tesla or Bruker Avance 16.4 Tesla vertical bore small animal
732 MRI system (Bruker Biospin, Billerica, MA)[65]. Gadolinium (Multihance-Bracco) was
733 administered intraperitoneally (100µL of 100mg/kg) ~15 minutes before scans. 25 mm and 34
734 mm volumetric coils were utilized. Animals were anesthetized with continuous isoflurane
735 administered through nose cone. Respiration and heart rate were monitored with an MRI
736 compatible vitals monitoring system (model 1030; SA Instruments, Stony Brook, NY).
737 After axial and sagittal tripilot positioning scans, isotropic 3D T1-weighted scans were employed
738 to detect gadolinium, with an approximate scan time of 30 minutes. Maximum intensity
739 projection scans were performed to detect gadolinium, with an approximate scan time of 10
740 minutes. Scoring was performed by two independent observers, blinded to genotype with <10%
741 intra-observer variation found. Analyze12.0 software (Biomedical Imaging Resource; Mayo
742 Clinic, Rochester, MN) was employed to analyze T1 data and to generate 3D maps of
743 gadolinium enhancement. Maximum intensity projection data was analyzed using Fiji Is Just
744 ImageJ (FIJI) 2.3.0; Java 1.8.0_172.
745
746 **Immunofluorescence**. Brains used for immunofluorescence staining were either fresh frozen or
747 paraformaldehyde fixed following mouse euthanasia and transcardial perfusion with ice-cold
748 PBS. Brains harvested after 2-photon imaging and FITC-albumin injection were harvested
749 without perfusion and paraformaldehyde fixed. All brain tissues were embedded in Tissue-Tek

750 OCT Compound, frozen on dry ice and sliced on cryostat with the exception of FITC-albumin
751 injected brains which were embedded in 4% agarose and sliced with vibratome. All brain slices
752 were mounted on SuperFrost Plus microscope slides and stored at 4 degrees.
753
754 **Single-cell suspension.** Mice were euthanized via isoflurane per IACUC guidelines and
755 transcardially perfused with ice-cold PBS. Brains and meninges were harvested and processed as
756 previously described[66, 67], via dounce homogenization and 30% Percoll gradient or enzymatically
757 digested using mouse tumor dissociation kit and gentleMACS™ Octo Dissociator (Miltenyi
758 Biotec). Spleens and lymph nodes were either digested with Collagenase IV/DNAse or not
759 digested before mechanical disruption. Lymph nodes were dissociated using frosted glass slides
760 and spleens were dissociated through 70 μM filter. Thymus samples were processed using
761 mechanical disruption through 70 μM filter. Blood was collected (100μl) into 1 mL heparin
762 (100U/mL). Spleens underwent ACK RBC lysis for 3 minutes and blood samples for 1minute.
763 All samples were filtered using 70 μM filters before counting, staining and running on flow
764 cytometer.
765
766 **Flow cytometry.** After resuspension in PBS, cells were either first stained with either Zombie
767 UV or Zombie NIR fixable viability dyes (BioLegend) (1:1000) for 20 minutes at room
768 temperature in the dark or Ghost Red 780 Viability dye (Tonbo) was added to surface stain
769 master mix. Samples underwent Fc-receptor block and staining for 30 minutes at 4 degrees with
770 surface staining antibodies. Panels requiring intracellular staining were then fixed and
771 permeabilized using Cyto-Fast™ Fix/Perm Buffer Set (BioLegend), and then stained with
772 intracellular antibodies for 30 minutes at room temperature in the dark before washing. All flow

773 panel staining was performed with this method with the exception of Annexin staining, which
774 required staining in Annexin V Binding Buffer (Invitrogen) for 15 minutes at room temperature
775 prior to fixation and permeabilization and intracellular staining. The antibodies that are specific
776 for surface markers included CD103 Brilliant Violet 421 (121422; BioLegend), NK1.1 Pac Blue
777 (108722; BioLegend), B220 Pac Blue (103227; BioLegend), CD62L Brilliant Violet 480
778 (746726; BD Biosciences), CD11b VioGreen (130-113-239; Miltenyi Biotec), CD44 Brilliant
779 Violet 570 (103037; BioLegend), CD80 Brilliant Violet 605 (104729; BioLegend), Ly6C
780 Brilliant Violet 650 (128049; BioLegend), H-2K^b/H-2D^b Brilliant Violet 750 (746869; BD
781 Biosciences), CCR7 Brilliant Violet 785 (120127; BioLegend), I-A/I-E BB515 (565254; BD
782 Biosciences), CD8a Spark Blue 550 (100780; BioLegend), CD45 PerCP (103130; BioLegend),
783 Ly6G PerCP-eFluor 710 (46-9668-82; Invitrogen), OX40L PE-Dazzle 594 (108816;
784 BioLegend), CD40 PE-Cy5 (124618; BioLegend), CD31 PE-Cy7 (25-0311-82; Invitrogen), CD3
785 Spark NIR 685 (100262; BioLegend), CD11c Alexa Fluor 700 (117320; BioLegend), CD4 APC-
786 Fire 750 (100568; BioLegend), CD25 Brilliant Violet 421 (102034; BioLegend), TCRβ APC
787 (20-5961-U100; Tonbo biosciences), c-kit Brilliant Violet 786 (564012; BD Biosciences), CD69
788 Brilliant Violet 650 (740460; BD Biosciences), Ly51 FITC (108305; BioLegend), EpCAM PE-
789 Cy7 (118216; BioLegend), CD8a Pac Blue (563898; BD Biosciences), CD4 APC (100516;
790 BioLegend), CD11a PE (141006; BioLegend), CD16/CD32 (553141; BD Pharmingen), Thy1.2
791 Alexa Fluor 488 (105316; BioLegend), I-A/I-E Pac Blue (107620; BioLegend), CD8a Brilliant
792 Violet 510 (100751; BioLegend), CD44 Brilliant Violet 650 (740455; BD Biosciences), Ly6G
793 Brilliant Violet 711 (46-9668-82; Invitrogen), CD4 Brilliant Violet 786 (563727; BD
794 Biosciences), Ly6C PerCP (128027; BioLegend), CD45 PE-CE594 (562420; BD Horizon),
795 CD11b PE-Cy5 (55-0112-U100; Tonbo biosciences), TCRβ PE-Cy7 (60-5961-U100; Tonbo

796 biosciences), B220 Spark NIR 685 (103268; BioLegend), CD62L APC-Fire 750 (104450;
797 BioLegend), CD11c Brilliant Violet 605 (117333; BioLegend), Annexin V(25-8103-72;
798 Invitrogen), B220 APC-Fire 810 (103277; BioLegend), CD26 Brilliant Violet 605 (745125; BD
799 Biosciences), CD80 Brilliant Violet 711 (104743; BioLegend), I-A/I-E Brilliant Violet 786
800 (743875; BD Biosciences), CD8a Brilliant Violet 421 (563898; BD Biosciences), CD31 APC-
801 Fire 750 (102528; BioLegend), CD11a PE-Cy7 (101122; BioLegend), CD31 PE-Dazzle
802 (102526; BioLegend), CXCR3 Brilliant Violet 421 (126521; BioLegend), CD106 Alexa Fluor
803 647 (105712; BioLegend), CD62P PE (148306; BioLegend), CD54 Brilliant Violet 711 (116143;
804 BioLegend), CD8 Brilliant Violet 570 (100740; BioLegend), Zombie NIR viability dye (Cat.
805 #423105; BioLegend), Zombie UV (423107; BioLegend). To assess cytokine production cells
806 were stained with intracellular markers after fixation and permeabilization: NeuN APC (100920;
807 Novus), IFNγ Brilliant Violet 785 (563773; BD Biosciences), IFNγ APC (20-7311-U100; Tonbo
808 biosciences) IL-12 PE (505204; BioLegend), IFNγ PE (50-7311-U100; Tonbo Biosciences). In
809 noted experiments, intravenous injection of 2ug of Thy1.2 Alexa Fluor 488 were administered 3
810 min. before collecting tissues to label T cells in vasculature. All samples were acquired on Cytek
811 Aurora spectral flow cytometer (Cytek, Fremont, CA). All analysis was performed using FlowJo
812 software version 10.8.1(FlowJo LLC, Ashland, OR).
813
814 ***In vivo* two-photon microscopy.** Mice were intravenously injected with 2 µg of Thy1.2 Alexa
815 Fluor 488 just prior to cranial window surgery, approximately 30 min prior to imaging. Cranial
816 windows were implanted as described [68 69]. In brief, under isoflurane anesthesia (3% induction,
817 1.5–2% maintenance), a circular craniotomy (<5 mm diameter) was made over somatosensory
818 cortex with the center at about -2.5 posterior and +2 lateral to bregma. A circular glass coverslip

819 (5 mm diameter, Warner) was secured over the craniotomy using dental cement (Tetric
820 EvoFlow). A four-point headbar (NeuroTar) was secured over the window using dental cement.
821 Mice were injected intravenously with intravascular dye 70,000 MW Dextran-Texas Red
822 (Invitrogen, D1830) 5 minutes before imaging. Alexa Fluor 488 (T cells) and Dextran-Texas
823 Red (vessels) were excited by a tunable Ti:Sapphire Mai Tai DeepSee laser (Spectra Physics,
824 CA, USA) at 940 nm and the emission was collected at 525/50 and 630/75 nm, respectively (U-
825 MF2, Olympus, Japan). An Olympus LUMPLFLN 40x water-immersion objective was used to
826 acquire image stacks. A 30-μm stack with 2 μm z-resolution and 512 × 512 pixels were acquired
827 every minute for a period of 10-30 min. Images were analyzed by Fiji ImageJ [70]. To analyze T
828 cell velocity, each 30-μm stack was first aligned along the z axis using the StackReg plugin
829 (Rigid Body) and Z-project into one image. Then images of every minute were stacked and
830 aligned using StackReg plugin (translation). The T cell velocity was measured using the Manual
831 Tracking plugin tracing for 10 min per field. The arrest coefficient is the percentage of each track
832 that a cell is immobile (instantaneous velocity <2 μm/min) [71].
833
834 **Parabiosis:** Procedure was performed as previously described. In brief, two female age-matched
835 mice of similar weight were selected. Mice were either littermates or co-housed for two weeks
836 prior to surgery. Anesthesia was induced and maintained with Ketamine/Xylazine (100/10
837 mg/kg; maintenance dose 30/3 mg/kg). Ophthalmic ointment was placed on eyes. Mice are tested
838 for reflex responses to ensure anesthetic depth. For analgesia during surgery, we administered
839 Carprofen and Buprenorphine-SR subcutaneously (5 mg/kg and 1 mg/kg). Animals were shaved
840 on the flank and prepped for surgery with Betadine swabs and sterile drapes. Using a sharp
841 scissor, superficial epidermal incision was continuously made along the flank starting at 0.5 cm

842 rostral of olecranon to 0.5 cm superior to patella. Skin absorbable 3-0 silk suture were used to
843 join elbow and knee joints (Ethicon Inc, Somerville, NJ). Simple continuous suture was
844 performed with absorbable 4-0 vicryl suture (Ethicon Inc, Somerville, NJ) for closer of incision.
845 Post-operatively we administer 1 ml of 0.9% NaCl fluids subcutaneous, analgesics Carprofen
846 intraperitoneally and Buprenorphine SR subcutaneously. Mice were placed on heating pad and
847 observed for a minimum of 3 hours after surgery. Prophylactically, mice were treated with
848 antibiotic Enrofloxacin (50 mg/kg) 10 days post-operatively. Parabiont pairs underwent a
849 minimum of 3 weeks of healing and acclimation time before experimental use. Procedure was
850 performed according to the IACUC guidelines at Mayo Clinic.
851
852 **Nanostring**. Brain dissections were subjected to RNA extraction (Qiagen RNAeasy Mini Kit Cat.
853 No. 74104), followed by nanodrop concentration and purity analysis. RNA samples were applied
854 to NanoString nCounter (NanoString Technologies, Seattle, WA) digital RNA quantification,
855 using the predesigned mouse Glial Profiling Panel codeset. The Glial Profiling Panel reagents were
856 provided by Nanostring. Reporter CodeSet Lot#RC8131X1. Capture Codeset Lot#CP8131X1.
857 Nanostring analysis was performed by the Thompson Lab at the Mayo Clinic Comprehensive
858 Cancer Center at Mayo Clinic Florida. Briefly, 100 ng of total RNA was hybridized to capture-
859 reporter probe codesets and immobilized on NanoString cartridges. Excess RNA and probes were
860 removed, and digital barcodes were counted. NanoString nCounter analysis software (v4.0) was
861 used for counting, quality control, and normalization. Transcript counts were normalized
862 according to NanoString's recommendations. Normalization parameters were applied with
863 normalization cutoff of 10. All samples were quality checked for quality and concentration. 13

housekeeping genes, 6 positive control genes, and 8 negative control genes were utilized for normalization.

Human brain microvascular endothelial cells

Human brain endothelial cell microarray data available through public repository at Gene Expression Omnibus (GEO), accession number GSE9861. Outlined in the publication by Tripathi et al, HBMECs were isolated from human brain specimens and characterized as described previously[19, 72]. In brief, HBMECs (passage < 6) from single adult donor were used for the biologic replicate experiments. For microarray experiments, HBMECs were grown in collagen-coated 6-well plates until cells achieved about 80% to 90% confluence. The medium was then changed to RPMI 1640 with 5% fetal bovine serum for 24 hours before coincubation with Pf-IRBCs, at which time HBMECs are confluent. Endothelial cells mycoplasma infection negative (Vector Laboratories).

Gene Expression Analyses. Human microarray data with accession number GSE9861[19] was utilized via Gene Expression Omnibus (GEO), a public functional genomics data repository supporting MIAME-compliant data submissions. Genes from human and mouse datasets were identified to be differentially expressed from each in comparison to a control group using either Ingenuity Pathway Analysis software (Qiagen), or Geo2R[73]. Gene set enrichment analysis (GSEA) was also performed on human data[74].

Statistics. When comparing results from two groups, an unpaired Student's t-test was used. When comparing results from two groups of paired mice, a paired Student's t-test was used.

When comparing results from three groups, a one-way analysis of variance (ANOVA) using Tukey's post-hoc multiple comparisons test was used. A two-way ANOVA when comparing statistically significant difference between the means of three or more independent groups that have been split on two variables, a two-way ANOVA using Šidák's multiple comparisons test was used. All statistical analyses were performed using Prism 6.0 (GraphPad Software) or Excel. Data are presented as the mean ± SD. and All p-values are shown or ns for non-significant p-value ($p > 0.05$).

Acknowledgments: We would like to thank Dr. Vanda Lennon for her feedback, Dr. Emma Goddery and Dr. Roman Khadka for discussions and Ryan Meloche for assisting with logistics of dual MRI. Some graphics were prepared on Biorender.com. Tetramers were provided by the NIH tetramer facility. **Funding sources:** R01NS103212 (AJJ), RF1NS122174 (AJJ), and F31NS116924 (CEF), R01AI167847 (JTH), Nanostring-Glial Panel Grant (CEF).

Financial disclosures: We have no financial interests to disclose.

Supplementary Table Figure Legends

Supplementary Table 1. IPA Causal network analysis identifies MHC Class I family as the number one master regulator of experimental cerebral malaria pathology. Causal network analysis was performed using the Ingenuity Pathway Analysis application. Table includes normalized data from causal network analysis which identifies master regulators of the most highly enriched signaling pathways in the Nanostring dataset comparing uninfected C57BL/6 brain vs. C57BL/6 brains with ECM. Master regulators of causal networks are listed in order of significance, with MHC Class I family identified as most significant causal network of experimental cerebral malaria pathology. P-value of overlap was adjusted using the Benjamini-Hochberg correction method.

Supplementary Table 2. Differentially expressed genes in human endothelial cells after *Plasmodium* infection exposure. Using GEO2R analysis platform MHC Class I was identified as one of the most significantly differentially expressed genes and was in the top 5 genes with significant upregulation on HBMECs after *Plasmodium* infection. Listed in order of significance.

Supplementary Table 3. Patterns of neuroinflammation determined by cell specific gene enrichment during ECM determined through Mouse Glial Profiling Panel. Table includes the nCounter Mouse Glial Profiling Panel gene lists, probes and corresponding cell type annotations detailing gene expression patterns and their corresponding neuroinflammatory response types.

References

1. Organization, W.H. World malaria report 2017. Geneva: WHO; 2017. 2018.

2. Organization, W.H. World malaria report 2021. (2021).

3. Idro, R., Marsh, K., John, C.C. & Newton, C.R. Cerebral malaria: mechanisms of brain injury and strategies for improved neurocognitive outcome. *Pediatr Res* **68**, 267-274 (2010).

4. Severe and complicated malaria. World Health Organization, Division of Control of Tropical Diseases. *Trans R Soc Trop Med Hyg* **84 Suppl 2**, 1-65 (1990).

5. Mahmoudi, S. & Keshavarz, H. Efficacy of phase 3 trial of RTS, S/AS01 malaria vaccine: The need for an alternative development plan. *Human vaccines & immunotherapeutics* **13**, 2098-2101 (2017).

6. Matuschewski, K. Vaccines against malaria—still a long way to go. *The FEBS journal* **284**, 2560-2568 (2017).

7. Rowe, A.K. *et al.* The burden of malaria mortality among African children in the year 2000. *Int J Epidemiol* **35**, 691-704 (2006).

8. Misra, U. *et al.* Cerebral malaria and bacterial meningitis. *Annals of Indian Academy of Neurology* **14**, S35 (2011).

9. Tunon-Ortiz, A. & Lamb, T.J. Blood brain barrier disruption in cerebral malaria: Beyond endothelial cell activation. *PLoS Pathogens* **15**, e1007786 (2019).

10. Seydel, K.B. *et al.* Brain swelling and death in children with cerebral malaria. *New England Journal of Medicine* **372**, 1126-1137 (2015).

11. Riggle, B.A. *et al.* CD8+ T cells target cerebrovasculature in children with cerebral malaria. *The Journal of clinical investigation* **130**, 1128-1138 (2020).

12. Ghazanfari, N., Mueller, S.N. & Heath, W.R. Cerebral malaria in mouse and man. *Frontiers in immunology* **9** (2018).

13. Finley, R., Mackey, L. & Lambert, P. Virulent P. berghei malaria: prolonged survival and decreased cerebral pathology in cell-dependent nude mice. *The Journal of Immunology* **129**, 2213-2218 (1982).

14. Yañez, D.M., Manning, D.D., Cooley, A.J., Weidanz, W.P. & Van Der Heyde, H. Participation of lymphocyte subpopulations in the pathogenesis of experimental murine cerebral malaria. *The Journal of Immunology* **157**, 1620-1624 (1996).

15. Nitcheu, J. *et al.* Perforin-dependent brain-infiltrating cytotoxic CD8+ T lymphocytes mediate experimental cerebral malaria pathogenesis. *The Journal of Immunology* **170**, 2221-2228 (2003).

16. Huggins, M.A. *et al.* Perforin expression by CD8 T cells is sufficient to cause fatal brain edema during experimental cerebral malaria. *Infection and immunity* **85**, e00985-00916 (2017).

17. Swanson, P.A. *et al.* CD8+ T cells induce fatal brainstem pathology during cerebral malaria via luminal antigen-specific engagement of brain vasculature. *PLoS pathogens* **12**, e1006022 (2016).

18. Takada, K. & Jameson, S.C. Self–class I MHC molecules support survival of naive CD8 T cells, but depress their functional sensitivity through regulation of CD8 expression levels. *Journal of Experimental Medicine* **206**, 2253-2269 (2009).

19. Tripathi, A.K., Sha, W., Shulaev, V., Stins, M.F. & Sullivan, D.J., Jr. Plasmodium falciparum-infected erythrocytes induce NF-kappaB regulated inflammatory pathways in human cerebral endothelium. *Blood* **114**, 4243-4252 (2009).

1001 20. Combes, V. *et al.* Pathogenic role of P-selectin in experimental cerebral malaria:
1002 importance of the endothelial compartment. *The American journal of pathology* **164**, 781-
1003 786 (2004).
1004
1005 21. Goddery, E.N. *et al.* Microglia and perivascular macrophages act as antigen presenting
1006 cells to promote CD8 T cell infiltration of the brain. *Frontiers in immunology*, 3428
1007 (2021).
1008
1009 22. Suidan, G.L., Mcdole, J.R., Chen, Y., Pirko, I. & Johnson, A.J. Induction of blood brain
1010 barrier tight junction protein alterations by CD8 T cells. *PloS one* **3**, e3037 (2008).
1011
1012 23. Pavelko, K.D. *et al.* Theiler's murine encephalomyelitis virus as a vaccine candidate for
1013 immunotherapy. *PloS one* **6**, e20217 (2011).
1014
1015 24. Campanella, G.S. *et al.* Chemokine receptor CXCR3 and its ligands CXCL9 and
1016 CXCL10 are required for the development of murine cerebral malaria. *Proceedings of the*
1017 *National Academy of Sciences* **105**, 4814-4819 (2008).
1018
1019 25. Ghazanfari, N., Mueller, S.N. & Heath, W.R. Cerebral malaria in mouse and man.
1020 *Frontiers in immunology*, 2016 (2018).
1021
1022 26. Cupovic, J. *et al.* Central nervous system stromal cells control local CD8+ T cell
1023 responses during virus-induced neuroinflammation. *Immunity* **44**, 622-633 (2016).
1024
1025 27. Zhao, H. *et al.* Olfactory plays a key role in spatiotemporal pathogenesis of cerebral
1026 malaria. *Cell host & microbe* **15**, 551-563 (2014).
1027
1028 28. Rai, D., Pham, N.-L.L., Harty, J.T. & Badovinac, V.P. Tracking the total CD8 T cell
1029 response to infection reveals substantial discordance in magnitude and kinetics between
1030 inbred and outbred hosts. *The Journal of Immunology* **183**, 7672-7681 (2009).
1031
1032 29. Bhat, P., Leggatt, G., Waterhouse, N. & Frazer, I.H. Interferon-γ derived from cytotoxic
1033 lymphocytes directly enhances their motility and cytotoxicity. *Cell death & disease* **8**,
1034 e2836-e2836 (2017).
1035
1036 30. Krasemann, S. *et al.* The TREM2-APOE pathway drives the transcriptional phenotype of
1037 dysfunctional microglia in neurodegenerative diseases. *Immunity* **47**, 566-581. e569
1038 (2017).
1039
1040 31. Keren-Shaul, H. *et al.* A unique microglia type associated with restricting development of
1041 Alzheimer's disease. *Cell* **169**, 1276-1290. e1217 (2017).
1042
1043 32. Aguzzi, A., Barres, B.A. & Bennett, M.L. Microglia: scapegoat, saboteur, or something
1044 else? *Science* **339**, 156-161 (2013).
1045

33. Deczkowska, A. *et al.* Disease-associated microglia: a universal immune sensor of neurodegeneration. *Cell* **173**, 1073-1081 (2018).

34. Pais, T.F. & Penha-Gonçalves, C. Brain endothelium: the "innate immunity response hypothesis" in cerebral malaria pathogenesis. *Frontiers in immunology* **9**, 3100 (2019).

35. Carman, C.V. & Martinelli, R. T lymphocyte–endothelial interactions: emerging understanding of trafficking and antigen-specific immunity. *Frontiers in immunology* **6**, 603 (2015).

36. Waisman, A. & Johann, L. Antigen-presenting cell diversity for T cell reactivation in central nervous system autoimmunity. *Journal of Molecular Medicine* **96**, 1279-1292 (2018).

37. Amersfoort, J., Eelen, G. & Carmeliet, P. Immunomodulation by endothelial cells—partnering up with the immune system? *Nature Reviews Immunology*, 1-13 (2022).

38. Murphy, K. & Weaver, C. *Janeway's immunobiology*. Garland science, 2016.

39. Engelhardt, B. & Ransohoff, R.M. The ins and outs of T-lymphocyte trafficking to the CNS: anatomical sites and molecular mechanisms. *Trends in immunology* **26**, 485-495 (2005).

40. Laschinger, M. & Engelhardt, B. Interaction of α4-integrin with VCAM-1 is involved in adhesion of encephalitogenic T cell blasts to brain endothelium but not in their transendothelial migration in vitro. *Journal of neuroimmunology* **102**, 32-43 (2000).

41. Marchetti, L. & Engelhardt, B. Immune cell trafficking across the blood-brain barrier in the absence and presence of neuroinflammation. *Vascular Biology* **2**, H1-H18 (2020).

42. Sathiyanadan, K., Coisne, C., Enzmann, G., Deutsch, U. & Engelhardt, B. PSGL-1 and E/P-selectins are essential for T-cell rolling in inflamed CNS microvessels but dispensable for initiation of EAE. *European journal of immunology* **44**, 2287-2294 (2014).

43. Villegas-Mendez, A. *et al.* IFN-γ–producing CD4+ T cells promote experimental cerebral malaria by modulating CD8+ T cell accumulation within the brain. *The Journal of Immunology* **189**, 968-979 (2012).

44. Krausgruber, T. *et al.* Structural cells are key regulators of organ-specific immune responses. *Nature* **583**, 296-302 (2020).

45. Howland, S.W. *et al.* Brain microvessel cross-presentation is a hallmark of experimental cerebral malaria. *EMBO molecular medicine* **5**, 984-999 (2013).

1091 46. Belnoue, E. *et al.* Control of pathogenic CD8+ T cell migration to the brain by IFN-γ
1092 during experimental cerebral malaria. *Parasite immunology* **30**, 544-553 (2008).
1093
1094 47. Suidan, G.L. *et al.* CD8 T cell-initiated vascular endothelial growth factor expression
1095 promotes central nervous system vascular permeability under neuroinflammatory
1096 conditions. *The journal of immunology* **184**, 1031-1040 (2010).
1097
1098 48. Miyakoda, M. *et al.* Malaria-specific and nonspecific activation of CD8+ T cells during
1099 blood stage of Plasmodium berghei infection. *The Journal of Immunology* **181**, 1420-
1100 1428 (2008).
1101
1102 49. Poh, C.M., Howland, S.W., Grotenbreg, G.M. & Rénia, L. Damage to the blood-brain
1103 barrier during experimental cerebral malaria results from synergistic effects of CD8+ T
1104 cells with different specificities. *Infection and immunity* **82**, 4854-4864 (2014).
1105
1106 50. Kalkal, M. *et al.* A comprehensive study of epitopes and immune reactivity among
1107 Plasmodium species. *BMC microbiology* **22**, 1-14 (2022).
1108
1109 51. Pardy, R.D. *et al.* Analysis of the T cell response to Zika virus and identification of a
1110 novel CD8+ T cell epitope in immunocompetent mice. *PLoS pathogens* **13**, e1006184
1111 (2017).
1112
1113 52. Mora, J.R. & von Andrian, U.H. T-cell homing specificity and plasticity: new concepts
1114 and future challenges. *Trends in immunology* **27**, 235-243 (2006).
1115
1116 53. Ioannidis, L.J., Nie, C.Q. & Hansen, D.S. The role of chemokines in severe malaria: more
1117 than meets the eye. *Parasitology* **141**, 602-613 (2014).
1118
1119 54. Miu, J. *et al.* Chemokine gene expression during fatal murine cerebral malaria and
1120 protection due to CXCR3 deficiency. *The Journal of Immunology* **180**, 1217-1230
1121 (2008).
1122
1123 55. Strangward, P. *et al.* A quantitative brain map of experimental cerebral malaria
1124 pathology. *PLoS pathogens* **13**, e1006267 (2017).
1125
1126 56. Solouki, S. *et al.* TCR signal strength and antigen affinity regulate CD8+ memory T
1127 cells. *The Journal of Immunology* **205**, 1217-1227 (2020).
1128
1129 57. Tan, M. *et al.* T cell receptor binding affinity governs the functional profile of cancer-
1130 specific CD8+ T cells. *Clinical & Experimental Immunology* **180**, 255-270 (2015).
1131
1132 58. Irving, M. *et al.* Interplay between T cell receptor binding kinetics and the level of
1133 cognate peptide presented by major histocompatibility complexes governs CD8+ T cell
1134 responsiveness. *Journal of Biological Chemistry* **287**, 23068-23078 (2012).
1135

59. Martinez, R.J. & Evavold, B.D. Lower affinity T cells are critical components and active participants of the immune response. *Frontiers in immunology* **6**, 468 (2015).

60. Tau, G.Z., Cowan, S.N., Weisburg, J., Braunstein, N.S. & Rothman, P.B. Regulation of IFN-γ signaling is essential for the cytotoxic activity of CD8+ T cells. *The Journal of Immunology* **167**, 5574-5582 (2001).

61. Malo, C.S. *et al.* Non-equivalent antigen presenting capabilities of dendritic cells and macrophages in generating brain-infiltrating CD8+ T cell responses. *Nature communications* **9**, 1-13 (2018).

62. Tritz, Z.P. *et al.* Conditional Silencing of H-2Db Class I Molecule Expression Modulates the Protective and Pathogenic Kinetics of Virus-Antigen–Specific CD8 T Cell Responses during Theiler's Virus Infection. *The Journal of Immunology* **205**, 1228-1238 (2020).

63. Hortle, E. *et al.* KCC1 Activation protects Mice from the Development of Experimental Cerebral Malaria. *Scientific reports* **9**, 1-11 (2019).

64. Organization, W.H. & Control, C.f.D. *Basic malaria microscopy: tutor's guide*. World Health Organization, 2010.

65. Johnson, H.L. *et al.* CD8 T cell-initiated blood–brain barrier disruption is independent of neutrophil support. *The Journal of Immunology* **189**, 1937-1945 (2012).

66. Garcia, L.M.C., Kelcher, A.M.H., Malo, C.S. & Johnson, A.J. Superior isolation of antigen-specific brain infiltrating T cells using manual homogenization technique. *Journal of immunological methods* **439**, 23-28 (2016).

67. Rustenhoven, J. *et al.* Functional characterization of the dural sinuses as a neuroimmune interface. *Cell* **184**, 1000-1016. e1027 (2021).

68. Liu, Y.U. *et al.* Neuronal network activity controls microglial process surveillance in awake mice via norepinephrine signaling. *Nature neuroscience* **22**, 1771-1781 (2019).

69. Eyo, U.B. *et al.* P2Y12R-Dependent Translocation Mechanisms Gate the Changing Microglial Landscape. *Cell reports* **23**, 959-966 (2018).

70. Schindelin, J. *et al.* Fiji: an open-source platform for biological-image analysis. *Nature methods* **9**, 676-682 (2012).

71. Shakhar, G. *et al.* Stable T cell-dendritic cell interactions precede the development of both tolerance and immunity in vivo. *Nature immunology* **6**, 707-714 (2005).

72. Tripathi, A.K., Sullivan, D.J. & Stins, M.F. Plasmodium falciparum-infected erythrocytes increase intercellular adhesion molecule 1 expression on brain endothelium through NF-κB. *Infection and immunity* **74**, 3262-3270 (2006).

73. Barrett, T. *et al.* NCBI GEO: archive for functional genomics data sets—update. *Nucleic acids research* **41**, D991-D995 (2012).

74. Subramanian, A. *et al.* Gene set enrichment analysis: a knowledge-based approach for interpreting genome-wide expression profiles. *Proceedings of the National Academy of Sciences* **102**, 15545-15550 (2005).

Figure 1

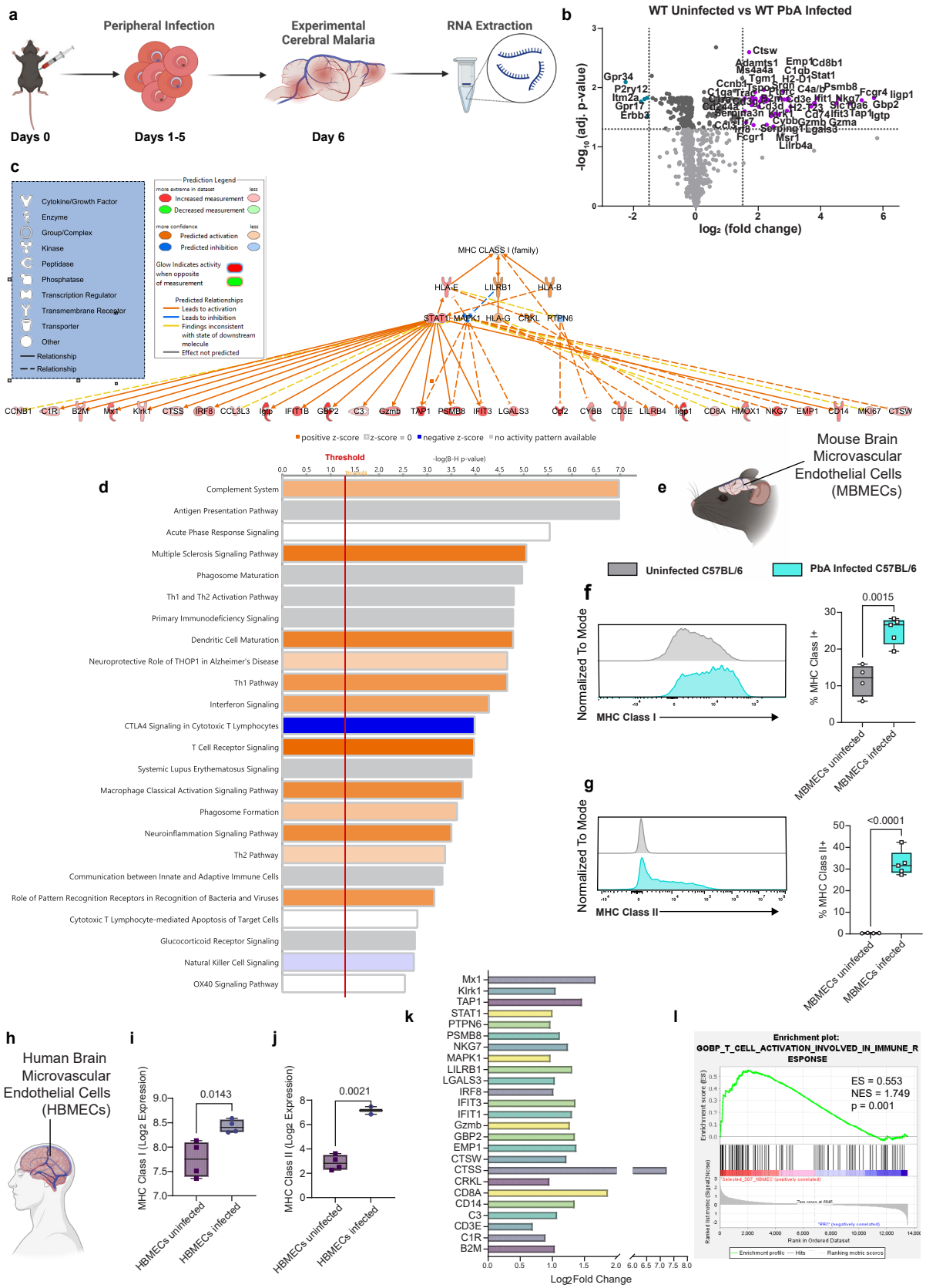
a
Peripheral Infection
Experimental Cerebral Malaria
RNA Extraction
Days 0
Days 1-5
Day 6
b
WT Uninfected vs WT PbA Infected
-log10 (adj. p-value)
log2 (fold change)
c
Prediction Legend
Cytokine/Growth Factor
Enzyme
Group/Complex
Kinase
Peptidase
Phosphatase
Transcription Regulator
Transmembrane Receptor
Transporter
Other
Relationship
Relationship
Increased measurement
Decreased measurement
Predicted activation
Predicted inhibition
Glow Indicates activity when opposite of measurement
Predicted Relationships
Leads to activation
Leads to inhibition
Findings inconsistent with state of downstream molecule
Effect not predicted
MHC CLASS I (family)
HLA-E
LILRB1
HLA-B
STAT1
MAPK1
HLA-G
CRKL
PTPN6
positive z-score
z-score = 0
negative z-score
no activity pattern available
d
Threshold
-log(B-H p-value)
Complement System
Antigen Presentation Pathway
Acute Phase Response Signaling
Multiple Sclerosis Signaling Pathway
Phagosome Maturation
Th1 and Th2 Activation Pathway
Primary Immunodeficiency Signaling
Dendritic Cell Maturation
Neuroprotective Role of THOP1 in Alzheimer's Disease
Th1 Pathway
Interferon Signaling
CTLA4 Signaling in Cytotoxic T Lymphocytes
T Cell Receptor Signaling
Systemic Lupus Erythematosus Signaling
Macrophage Classical Activation Signaling Pathway
Phagosome Formation
Neuroinflammation Signaling Pathway
Th2 Pathway
Communication between Innate and Adaptive Immune Cells
Role of Pattern Recognition Receptors in Recognition of Bacteria and Viruses
Cytotoxic T Lymphocyte-mediated Apoptosis of Target Cells
Glucocorticoid Receptor Signaling
Natural Killer Cell Signaling
OX40 Signaling Pathway
e
Mouse Brain Microvascular Endothelial Cells (MBMECs)
Uninfected C57BL/6
PbA Infected C57BL/6
f
Normalized To Mode
MHC Class I
% MHC Class I+
0.0015
MBMECs uninfected
MBMECs infected
g
Normalized To Mode
MHC Class II
% MHC Class II+
<0.0001
MBMECs uninfected
MBMECs infected
h
Human Brain Microvascular Endothelial Cells (HBMECs)
i
MHC Class I (Log2 Expression)
0.0143
HBMECs uninfected
HBMECs infected
j
MHC Class II (Log2 Expression)
0.0021
HBMECs uninfected
HBMECs infected
k
Mx1
Klrk1
TAP1
STAT1
PTPN6
PSMB8
NKG7
MAPK1
LILRB1
LGALS3
IRF8
IFIT3
IFIT1
Gzmb
GBP2
EMP1
CTSW
CTSS
CRKL
CD8A
CD14
C3
CD3E
C1R
B2M
Log2 Fold Change
l
Enrichment plot:
GOBP_T_CELL_ACTIVATION_INVOLVED_IN_IMMUNE_RESPONSE
ES = 0.553
NES = 1.749
p = 0.001
Enrichment score (ES)
Rank in Ordered Dataset
Enrichment profile
Hits
Ranking metric scores

Fig 1. Mouse and human brain microvascular endothelial cells become antigen presenting cells during cerebral malaria a) Flowchart showing steps of peripheral malaria infection, development of experimental cerebral malaria and RNA extraction for Nanostring analysis. b) Volcano plot of differentially expressed genes in whole brains of uninfected C57BL/6 mice versus PbA infected mice on day 6 of infection. Significantly upregulated genes are indicated on upper right (purple dots). Significantly downregulated genes are indicated on upper left (turquoise dots). Horizontal dotted line indicates cutoff of adjusted p-values (-Log10 of adjusted p-value 1.3 corresponding to a threshold of p-value of 0.05). Vertical dotted line indicates cutoff of log2 Fold change (-1.5 to 1.5). c) Ingenuity Pathway Analysis (IPA) was performed, and Causal network analysis identified MHC Class I family as the most significant network master regulator in experimental cerebral malaria pathology which led to the differential expression of the genes of interest. Depicted in c) a schematic of the homologous master regulator pathway and corresponding downstream genes. Coloring of the molecules corresponds to calculated z-scores (algorithm predicting activation or inhibition). Red indicates increased gene activation, orange indicates predicted activation of pathways, green indicates decreased gene activation, blue indicates predicted inhibition of pathways, white indicates a z-score of zero with equal evidence for activation and inhibition, grey indicates that z-score could not be calculated. d) Canonical pathway analysis identified significantly differential signaling pathways. P-value of overlap was adjusted using the Benjamini-Hochberg correction method. Bars are arranged in order of significance score with threshold (red line) set at p-value 0.05 (corresponding to a negative log value of 1.3). Coloring of bars corresponds to calculated z-scores (algorithm predicting activation or inhibition). Orange bars indicate activated pathways, blue indicates inhibited pathways, white indicates a z-score of zero with equal evidence for activation and inhibition, grey indicates that z-score could not be calculated. e) Schematic depicting C57BL/6 and naming convention of mouse brain microvascular endothelial cells (MBMECs). High-dimensional flow cytometry was performed on mouse brains on day 6 of PbA infection and uninfected age and sex matched controls. f) Representative histogram of MHC Class I expression on MBMECs and quantified frequency of MHC Class I high endothelial cells. g) Representative histogram of MHC Class II expression on MBMECs and quantified frequency. h) Schematic depicting human subjects and naming convention of human brain microvascular endothelial cells (HBMECs). i-j) Box plots depicting Log_2 expression data from human endothelial cells in published microarray (GEO Accession: GSE9861). i) MHC Class I Log_2 expression in control HBMECs vs. *Plasmodium* exposed HBMECs. j) MHC Class I Log_2 expression in control HBMECs vs. *Plasmodium* exposed HBMECs selected as highly activated (with high expression of adhesion molecules). k) Log_2 Fold change of genes of interest which lie downstream of the MHC class I signaling pathway in HBMECs during *Plasmodium* falciparum infection. GSEA was performed on HBMEC transcriptomic data. l) Enrichment plot showing enrichment of molecular signature for T cell activation involved in immune response pathway. The y-axis represents enrichment score (ES) and on the x-axis are genes (vertical black lines) represented in gene sets. The green line connects points of ES and genes. ES is the maximum deviation from zero as calculated for each gene going down the ranked list and represents the degree of over-representation of a gene set at the top or the bottom of the ranked gene list. The colored band at the bottom represents the degree of correlation of genes with the phenotype (red for positive and blue for negative correlation). Significance threshold set at nominal p-value < 0.05. Gene sets for T cell activation involved in immune response were significant only in HBMECs during infection. Data were

analyzed with unpaired t test (f, g, i, and j). Box plots present the mean $\pm$ SD. All p-values are shown or ns for non-significant p-value *($p > 0.05$)*.

Figure 2

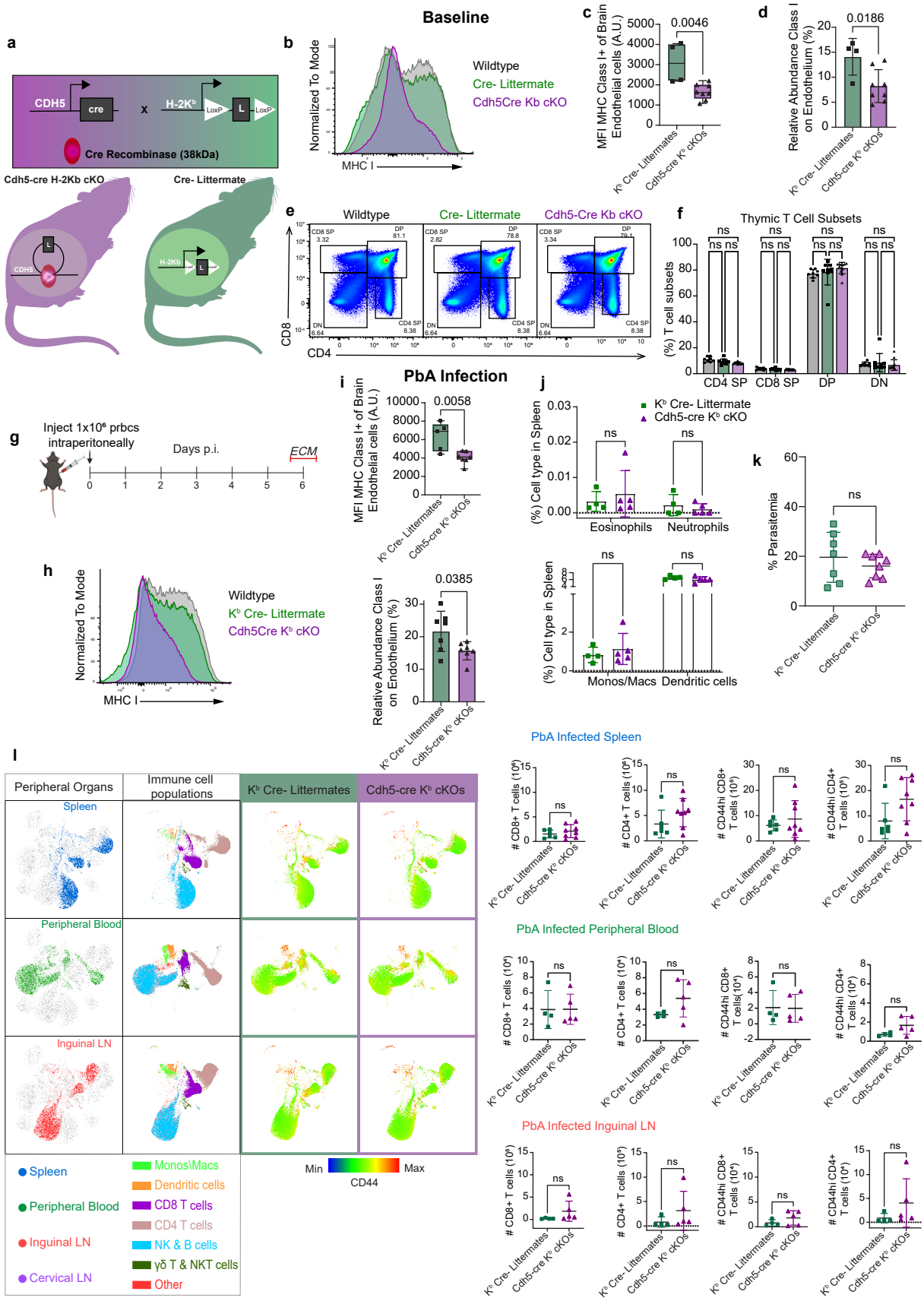
a
CDH5
cre
x
H-2Kb
LoxP
L
LoxP
Cre Recombinase (38kDa)
Cdh5-cre H-2Kb cKO
Cre- Littermate
b
Baseline
Normalized To Mode
MHC I
Wildtype
Cre- Littermate
Cdh5Cre Kb cKO
c
MFI MHC Class I+ of Brain Endothelial cells (A.U.)
0.0046
Kb Cre- Littermates
Cdh5-cre Kb cKOs
d
Relative Abundance Class I on Endothelium (%)
0.0186
e
Wildtype
Cre- Littermate
Cdh5-Cre Kb cKO
CD8
CD4
f
Thymic T Cell Subsets
(%) T cell subsets
CD4 SP
CD8 SP
DP
DN
ns
g
Inject 1x10⁶ prbcs intraperitoneally
Days p.i.
ECM
h
Wildtype
Kb Cre- Littermate
Cdh5Cre Kb cKO
i
PbA Infection
0.0058
0.0385
j
Kb Cre- Littermate
Cdh5-cre Kb cKO
(%) Cell type in Spleen
Eosinophils
Neutrophils
Monos/Macs
Dendritic cells
k
% Parasitemia
l
Peripheral Organs
Immune cell populations
Kb Cre- Littermates
Cdh5-cre Kb cKOs
Spleen
Peripheral Blood
Inguinal LN
Min
Max
CD44
Monos\Macs
Dendritic cells
CD8 T cells
CD4 T cells
NK & B cells
γδ T & NKT cells
Other
Cervical LN
PbA Infected Spleen
PbA Infected Peripheral Blood
PbA Infected Inguinal LN
CD8+ T cells
CD4+ T cells
CD44hi CD8+ T cells
CD44hi CD4+ T cells

Fig 2. Normal peripheral infection and immunity in mice with K^b class I molecule conditionally ablated on vasculature a) Schematic depicted Cre-LoxP strategy. Cdh5-Cre mice were crossed to transgenic H-2K^b LoxP mice. b) Representative MFI plot comparing C57BL/6, Cdh5-Cre K^b cKO, and Cre-Littermate expression of MHC I on brain endothelium in naïve mice. c) Quantification of MHC I MFIs on brain endothelial cells using arbitrary units (A.U.) in naïve mice. d) Percentage of brain endothelial cells expressing high levels of MHC Class I molecules in naïve mice. e) Representative flow plot of C57BL/6, Cdh5-Cre K^b cKO, and Cre-Littermate T cell subsets in thymus. f) Percentage of thymic T cell subsets. g) Schematic representing timeline of infection for development of ECM. h) Representative MFI plot comparing C57BL/6, Cdh5-Cre K^b cKO, and Cre-Littermate expression of MHC I on brain endothelium in PbA infected mice. i) Quantification of MHC I MFIs on brain endothelial cells using arbitrary units (A.U.) in PbA infected mice. j) Percentage of brain endothelial cells expressing high levels of MHC Class I molecules in PbA infected mice. k) Percentage of granulocytes in spleens of infected mice. l) Percentage of antigen-presenting cells in spleens of infected mice. m) Percent parasitemia quantified by imaging Giemsa-stained thin blood smears in PbA infected mice. n) Representative UMAPs depicting peripheral organs and immune cell populations and respective heats maps with CD44 activation marker expression. o) The scatter plots show quantified absolute cell counts of CD8 T cells, CD4 T cells and CD44hi CD8 T cells and CD4 T cells in the respective organs depicted in n). Data were analyzed with unpaired t test or 2way ANOVA with multiple comparisons. Scatterplots and bar plots present the mean $\pm$ SD. All p-values are shown or ns for non-significant p-value *($p > 0.05$)*.

Figure 3

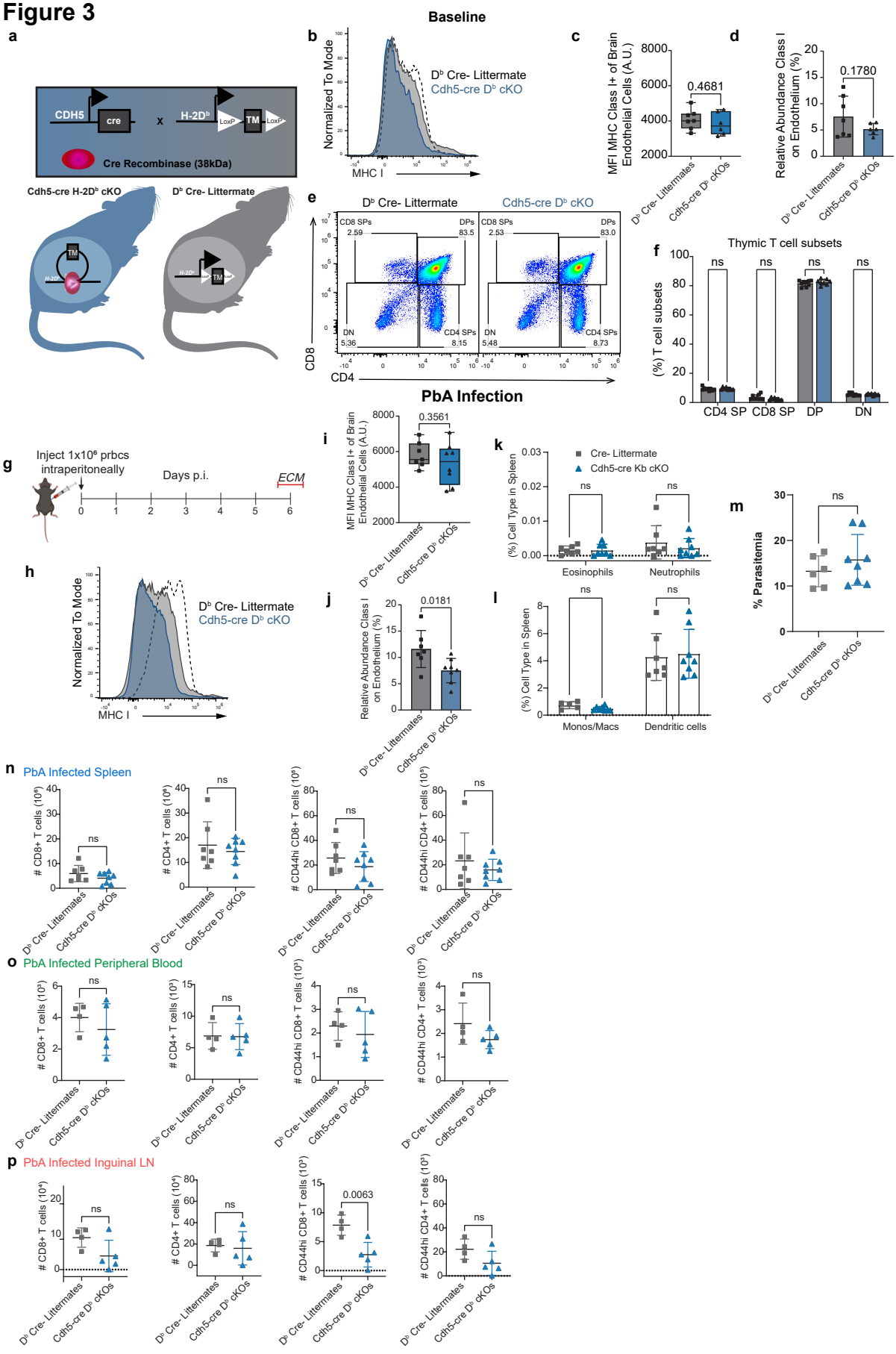
a
CDH5
cre
x
H-2Dᵇ
LoxP
TM
LoxP
Cre Recombinase (38kDa)
Cdh5-cre H-2Dᵇ cKO
Dᵇ Cre- Littermate
Baseline
b
Normalized To Mode
Dᵇ Cre- Littermate
Cdh5-cre Dᵇ cKO
MHC I
c
MFI MHC Class I+ of Brain Endothelial Cells (A.U.)
0.4681
Dᵇ Cre- Littermates
Cdh5-cre Dᵇ cKOs
d
Relative Abundance Class I on Endothelium (%)
0.1780
e
Dᵇ Cre- Littermate
Cdh5-cre Dᵇ cKO
CD8 SPs
DPs
DN
CD4 SPs
2.59
83.5
5.36
8.15
2.53
83.0
5.48
8.73
CD8
CD4
f
Thymic T cell subsets
(%) T cell subsets
ns
CD4 SP
CD8 SP
DP
DN
PbA Infection
g
Inject 1x10⁶ prbcs intraperitoneally
Days p.i.
ECM
h
i
0.3561
j
0.0181
k
Cre- Littermate
Cdh5-cre Kb cKO
(%) Cell Type in Spleen
Eosinophils
Neutrophils
l
Monos/Macs
Dendritic cells
m
% Parasitemia
n PbA Infected Spleen
CD8+ T cells (10⁴)
CD4+ T cells (10⁴)
CD44hi CD8+ T cells (10³)
CD44hi CD4+ T cells (10³)
o PbA Infected Peripheral Blood
p PbA Infected Inguinal LN
0.0063

Fig 3. Normal peripheral infection and immunity in mice with D^b class I molecule conditionally ablated on vasculature a) Schematic depicted Cre-LoxP strategy. Cdh5-Cre mice were crossed to transgenic H-2D^b LoxP mice. b) Representative MFI plot comparing C57BL/6, Cdh5-Cre D^b cKO, and Cre-Littermate expression of MHC I on brain endothelium in naïve mice. c) Quantification of MHC I MFIs on brain endothelial cells using arbitrary units (A.U.) in naïve mice. d) Percentage of brain endothelial cells expressing high levels of MHC Class I molecules in naïve mice. e) Representative flow plot of C57BL/6, Cdh5-Cre D^b cKO, and Cre-Littermate T cell subsets in thymus. f) Percentage of thymic T cell subsets. g) Schematic representing timeline of infection for development of ECM. h) Representative MFI plot comparing C57BL/6, Cdh5-Cre D^b cKO, and Cre-Littermate expression of MHC I on brain endothelium in PbA infected mice. i) Quantification of MHC I MFIs on brain endothelial cells using arbitrary units (A.U.) in PbA infected mice. j) Percentage of brain endothelial cells expressing high levels of MHC Class I molecules in PbA infected mice. k) Percentage of granulocytes in spleens. l) Percentage of antigen-presenting cells in spleens. m) Percent parasitemia quantified by imaging Giemsa-stained thin blood smears in PbA infected red blood cells. n) Scatter plots show quantified absolute cell counts of CD8 T cells, CD4 T cells and CD44hi CD8 T cells and CD4 T cells in spleen. o) Scatter plots show quantified absolute cell counts of CD8 T cells, CD4 T cells and CD44hi CD8 T cells and CD4 T cells in peripheral blood. p) Scatter plots show quantified absolute cell counts of CD8 T cells, CD4 T cells and CD44hi CD8 T cells and CD4 T cells in inguinal LN. Data were analyzed with unpaired t test or 2way ANOVA with multiple comparisons. Scatterplots and bar plots present the mean $\pm$ SD. All p-values are shown or ns for non-significant p-value *($p > 0.05$)*.

Figure 4

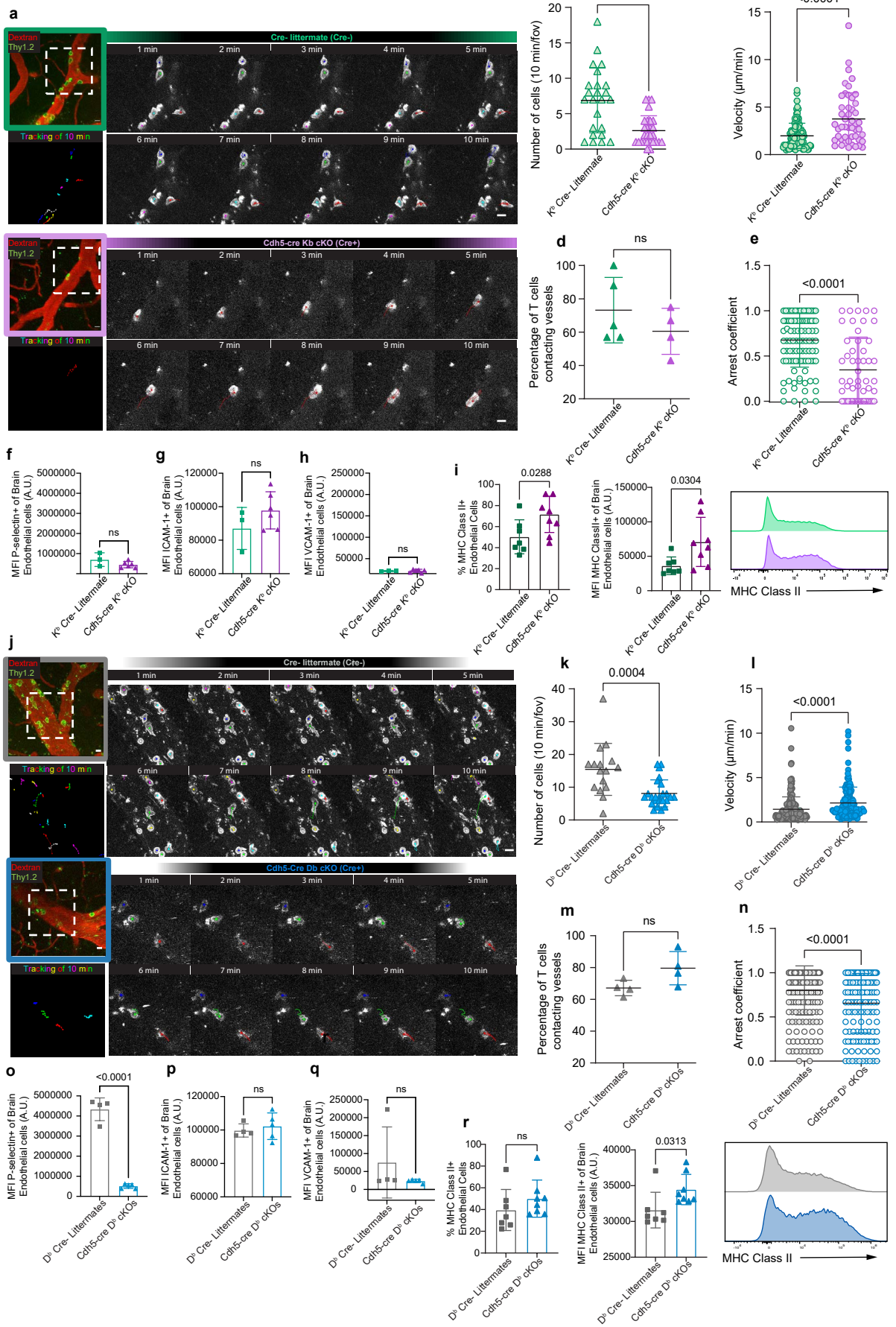
a
Dextran
Thy1.2
Cre- littermate (Cre-)
1 min
2 min
3 min
4 min
5 min
Tracking of 10 min
6 min
7 min
8 min
9 min
10 min
Cdh5-cre Kb cKO (Cre+)
b
0.0002
Number of cells (10 min/fov)
Kᵇ Cre- Littermate
Cdh5-cre Kᵇ cKO
c
<0.0001
Velocity (µm/min)
d
ns
Percentage of T cells contacting vessels
e
<0.0001
Arrest coefficient
f
MFI P-selectin+ of Brain Endothelial cells (A.U.)
g
MFI ICAM-1+ of Brain Endothelial cells (A.U.)
h
MFI VCAM-1+ of Brain Endothelial cells (A.U.)
i
0.0288
% MHC Class II+ Endothelial Cells
MFI MHC ClassII+ of Brain Endothelial cells (A.U.)
0.0304
MHC Class II
j
Cre- littermate (Cre-)
Cdh5-Cre Db cKO (Cre+)
Dᵇ Cre- Littermates
Cdh5-cre Dᵇ cKOs
k
0.0004
l
<0.0001
m
ns
n
<0.0001
o
<0.0001
p
ns
q
ns
r
ns
0.0313

Fig 4. T cell dynamics at brain vasculature are dependent on MHC class I expression during infection a) Representative images of T cells in brain vasculature with blood vessels labeled with I.V. Dextran-Texas ~5 min. prior to imaging and T cells I.V. labeled with anti-Thy1.2-Alexa Fluor 488 ~30 min. Inset is representative of T cell tracking over time through acute cranial window on days 6-7 post PbA infection. T cells (green) were visualized interacting with blood vessels (red) over periods of 10-30 min. Upper row represents K^b Cre- littermates and bottom row represents Cdh5-cre K^b cKO mice. Scale bar, 10 µM. b) Scatter plot represents numbers of T cells visualized over 10 min time periods/FOV. c) T cell velocity was measured using the Manual Tracking plugin in FIJI. Data are representative of µm/min over periods of 10 min per field and per cell. d) Percentage of T cells contacting vessels was calculated by obtaining the percent of all visualized T cells that contacted vasculature over many fields of view. Each data point is representative of the overall average percentage/mouse. e) The arrest coefficient is the percentage of each cell track that a cell is immobile (instantaneous velocity <2 µm/min). Each dot represents one cell and its percentage of contacts over time. (n = 5-7 mice per group). See corresponding S1-S5 movies. High-dimensional flow cytometry was performed to assess levels of protein expression on brain endothelium day 6 of PbA infection. f) Scatter plot represents MFI values of P-selectin on brain endothelial cells. g) MFI of ICAM-1on brain endothelial cells h) MFI of VCAM-1 on brain endothelial cells. i) Percentage and MFI quantification of MHC Class II molecules on brain endothelial cells with representative histogram. j) Representative images of T cells in brain vasculature labeled as described above. Inset is representative of T cell tracking over time through acute cranial window on days 6-7 post PbA infection. T cells (green) were visualized interacting with blood vessels (red) over periods of 10-30 min. Upper row represents D^b Cre- littermates and bottom row represents Cdh5-cre D^b cKO mice. Scale bar, 10 µM. k) Scatter plot represents numbers of T cells visualized over 10 min time periods/FOV. l) T cell velocity was measured using the Manual Tracking plugin in FIJI. Data are representative of µm/min over periods of 10 min per field and per cell. m) Percentage of T cells contacting vessels was calculated by obtaining the percent of all visualized T cells that contacted vasculature over many fields of view. Each data point is representative of the overall average percentage/mouse. n) The arrest coefficient is the percentage of each cell track that a cell is immobile (instantaneous velocity <2 µm/min). Each dot represents one cell and its percentage of contacts over time. (n = 5 mice per group). See corresponding S1-S5 movies. High-dimensional flow cytometry was performed to assess levels of protein expression on brain endothelium day 6 of PbA infection. o) Scatter plot represents MFI values of P-selectin on brain endothelial cells. p) MFI of ICAM-1on brain endothelial cells q) MFI of VCAM-1 on brain endothelial cells. r) Percentage and MFI quantification of MHC Class II molecules on brain endothelial cells with representative histogram. Data were analyzed with unpaired t test. Scatterplots and bar plots present the mean ± SD. All p-values are shown or ns for non-significant p-value *(p > 0.05)*.

Figure 5

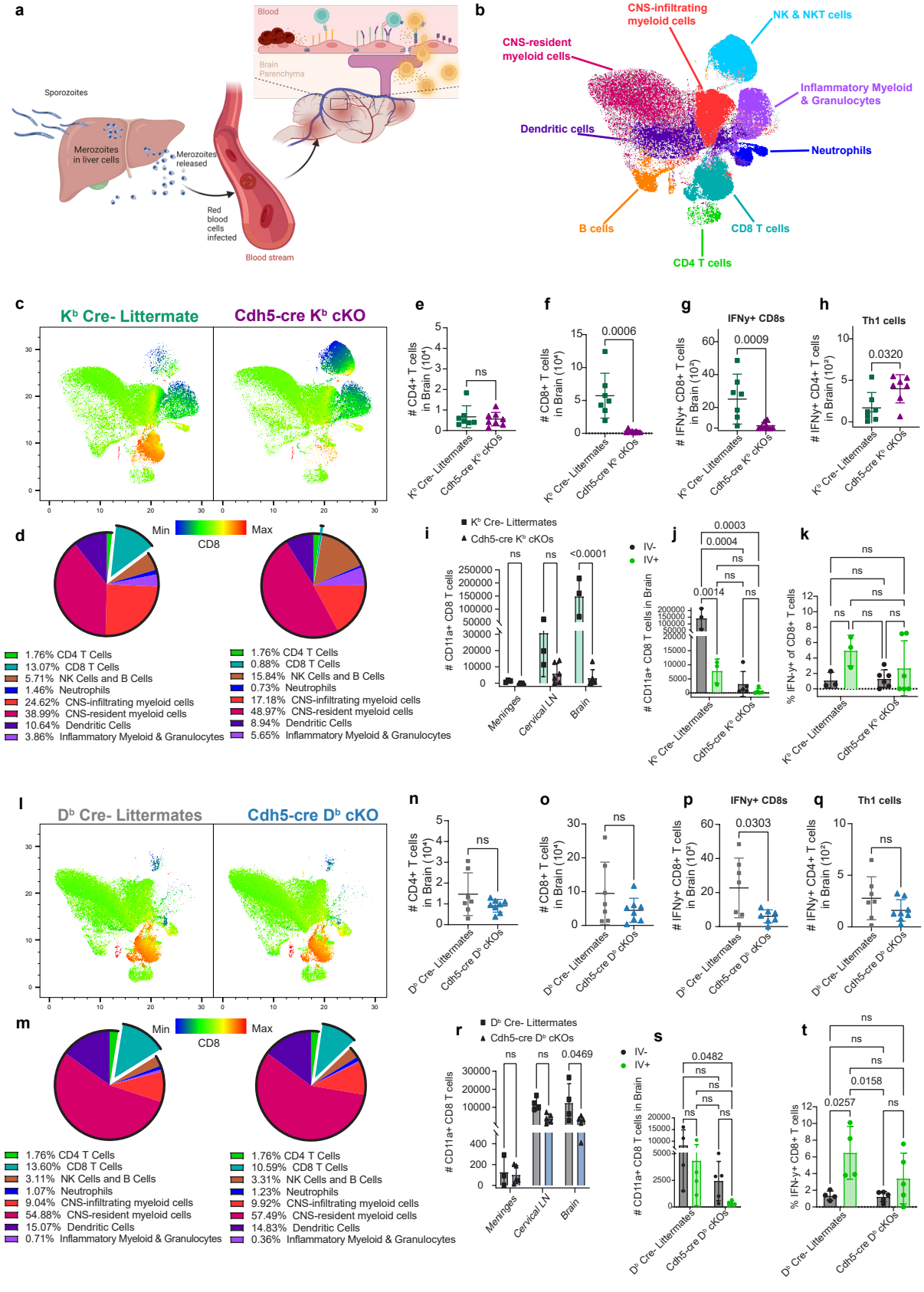
a
Blood
Brain Parenchyma
Sporozoites
Merozoites in liver cells
Merozoites released
Red blood cells infected
Blood stream
b
CNS-infiltrating myeloid cells
NK & NKT cells
CNS-resident myeloid cells
Inflammatory Myeloid & Granulocytes
Dendritic cells
Neutrophils
B cells
CD8 T cells
CD4 T cells
c
Kᵇ Cre- Littermate
Cdh5-cre Kᵇ cKO
d
Min
CD8
Max
1.76% CD4 T Cells
13.07% CD8 T Cells
5.71% NK Cells and B Cells
1.46% Neutrophils
24.62% CNS-infiltrating myeloid cells
38.99% CNS-resident myeloid cells
10.64% Dendritic Cells
3.86% Inflammatory Myeloid & Granulocytes
1.76% CD4 T Cells
0.88% CD8 T Cells
15.84% NK Cells and B Cells
0.73% Neutrophils
17.18% CNS-infiltrating myeloid cells
48.97% CNS-resident myeloid cells
8.94% Dendritic Cells
5.65% Inflammatory Myeloid & Granulocytes
e
CD4+ T cells in Brain (10⁴)
ns
Kᵇ Cre- Littermates
Cdh5-cre Kᵇ cKOs
f
CD8+ T cells in Brain (10⁴)
0.0006
g
IFNγ+ CD8s
IFNγ+ CD8+ T cells in Brain (10³)
0.0009
h
Th1 cells
IFNγ+ CD4+ T cells in Brain (10³)
0.0320
i
Kᵇ Cre- Littermates
Cdh5-cre Kᵇ cKOs
CD11a+ CD8 T cells
ns
ns
<0.0001
Meninges
Cervical LN
Brain
j
IV-
IV+
CD11a+ CD8 T cells in Brain
0.0003
0.0004
ns
0.0014
ns
k
% IFNγ+ of CD8+ T cells
ns
ns
ns
ns
ns
l
Dᵇ Cre- Littermates
Cdh5-cre Dᵇ cKO
m
Min
CD8
Max
1.76% CD4 T Cells
13.60% CD8 T Cells
3.11% NK Cells and B Cells
1.07% Neutrophils
9.04% CNS-infiltrating myeloid cells
54.88% CNS-resident myeloid cells
15.07% Dendritic Cells
0.71% Inflammatory Myeloid & Granulocytes
1.76% CD4 T Cells
10.59% CD8 T Cells
3.31% NK Cells and B Cells
1.23% Neutrophils
9.92% CNS-infiltrating myeloid cells
57.49% CNS-resident myeloid cells
14.83% Dendritic Cells
0.36% Inflammatory Myeloid & Granulocytes
n
CD4+ T cells in Brain (10⁴)
ns
Dᵇ Cre- Littermates
Cdh5-cre Dᵇ cKOs
o
CD8+ T cells in Brain (10⁴)
ns
p
IFNγ+ CD8s
IFNγ+ CD8+ T cells in Brain (10³)
0.0303
q
Th1 cells
IFNγ+ CD4+ T cells in Brain (10³)
ns
r
Dᵇ Cre- Littermates
Cdh5-cre Dᵇ cKOs
CD11a+ CD8 T cells
ns
ns
0.0469
Meninges
Cervical LN
Brain
s
IV-
IV+
CD11a+ CD8 T cells in Brain
0.0482
ns
ns
ns
ns
ns
t
% IFNγ+ of CD8+ T cells
ns
ns
ns
0.0158
0.0257
ns

Fig 5. Modulation of individual class I molecules on brain endothelium results in brain-specific CD8 T cell infiltration changes. a) BioRender schematic of events in the periphery leading up to cerebral malaria. b) Representative UMAP key, colorized to highlight the different cell subsets in the brain. c) Representative UMAPs of K^b Cre- Littermate and Cdh5-cre K^b cKO brains, colorized with heat map of CD8 expression. d) Pie charts with corresponding frequencies of cell subset in K^b Cre- Littermate and Cdh5-cre K^b cKO brains (of CD45+) e) Absolute counts of CD4 T cells in the brains of infected K^b Cre- Littermate and Cdh5-cre K^b cKO brains. f) Absolute counts of CD8 T cells in the brains of infected K^b Cre- Littermate and Cdh5-cre K^b cKO brains. g) Absolute counts of IFN-γ+ CD8 T cells in the brains of infected K^b Cre- Littermates and Cdh5-cre K^b cKOs. h) Absolute counts of IFN-γ+ CD4 T (Th1) cells in the brains of infected K^b Cre- Littermates and Cdh5-cre K^b cKOs. i) Absolute counts of CD11a+ (antigen-experienced) CD8 T cells in the meninges, cLN and brain of infected K^b Cre- Littermates and Cdh5-cre K^b cKOs. Mice were injected with Alexa Fluor 488-anti-Thy1.2 antibody ~3 min. before euthanasia. j) Quantified absolute counts of either IV+ or IV- antigen-experienced CD8 T cells in the brains of infected K^b Cre- Littermates and Cdh5-cre K^b cKOs. k) Frequency of IFN-γ+ CD8 T cells either labeled with IV antibody or negative for IV labeling. l) Representative UMAPs of D^b Cre- Littermate and Cdh5-cre D^b cKO brains, colorized with heat map of CD8 expression. m) Pie charts with corresponding frequencies of cell subset in D^b Cre- Littermate and Cdh5-cre D^b cKO brains (of CD45+) n) Absolute counts of CD4 T cells in the brains of infected D^b Cre- Littermate and Cdh5-cre D^b cKO brains. o) Absolute counts of CD8 T cells in the brains of infected D^b Cre- Littermate and Cdh5-cre D^b cKO brains. p) Absolute counts of IFN-γ+ CD8 T cells in the brains of infected D^b Cre- Littermates and Cdh5-cre D^b cKOs. q) Absolute counts of IFN-γ+ CD4 T (Th1) cells in the brains of infected D^b Cre- Littermates and Cdh5-cre D^b cKOs. r) Absolute counts of CD11a+ (antigen-experienced) CD8 T cells in the meninges, cLN and brain of infected D^b Cre- Littermates and Cdh5-cre D^b cKOs. Mice were injected with Alexa Fluor 488-anti-Thy1.2 antibody ~3 min. before euthanasia. s) Quantified absolute counts of either IV+ or IV- antigen-experienced CD8 T cells in the brains of infected D^b Cre- Littermates and Cdh5-cre D^b cKOs. t) Frequency of IFN-γ+ CD8 T cells either labeled with IV antibody or negative for IV labeling. Data were analyzed with unpaired t test or 2way ANOVA with multiple comparisons. Scatterplots and bar plots present the mean ± SD. All p-values are shown or ns for non-significant p-value *($p > 0.05$)*.

Figure 6

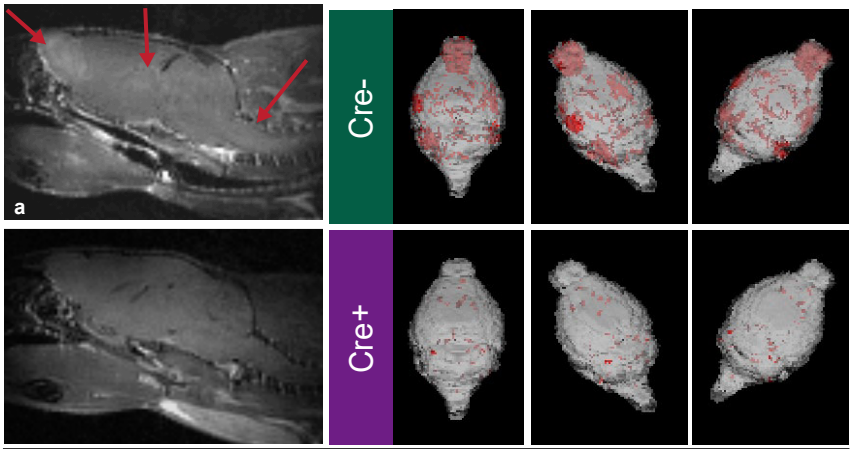
a
Cre-
Cre+

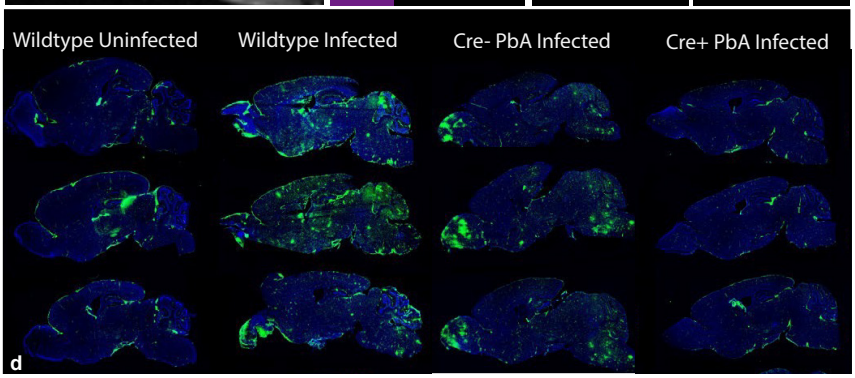
Wildtype Uninfected
Wildtype Infected
Cre- PbA Infected
Cre+ PbA Infected
d

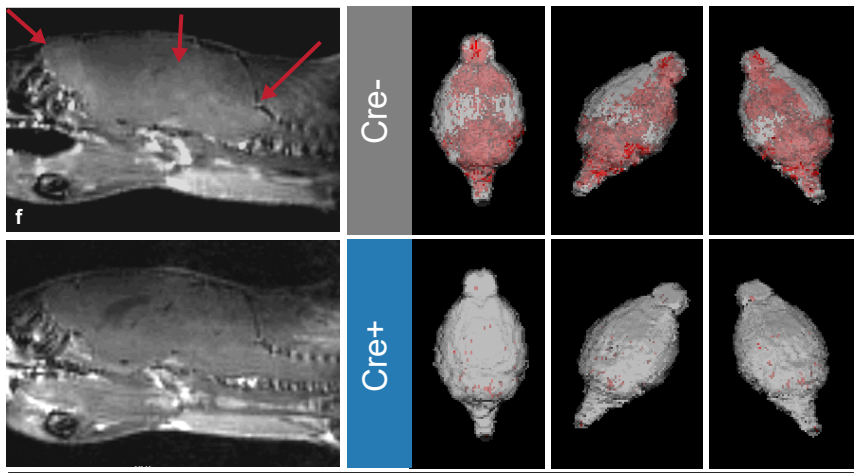
f
Cre-
Cre+

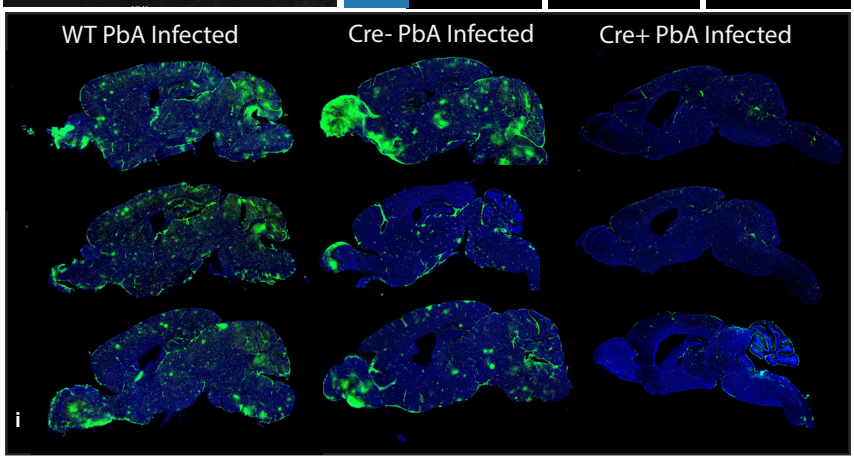
WT PbA Infected
Cre- PbA Infected
Cre+ PbA Infected
i

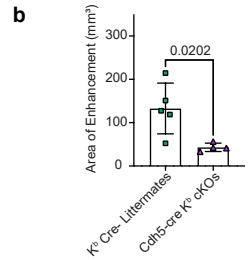
b
Area of Enhancement (mm³)
300
200
100
0
0.0202
Kᵇ Cre- Littermates
Cdh5-cre Kᵇ cKOs

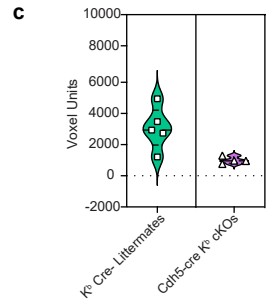
c
Voxel Units
10000
8000
6000
4000
2000
0
-2000
Kᵇ Cre- Littermates
Cdh5-cre Kᵇ cKOs

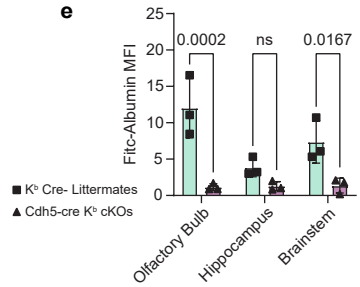
e
Fitc-Albumin MFI
25
20
15
10
5
0
0.0002
ns
0.0167
Kᵇ Cre- Littermates
Cdh5-cre Kᵇ cKOs
Olfactory Bulb
Hippocampus
Brainstem

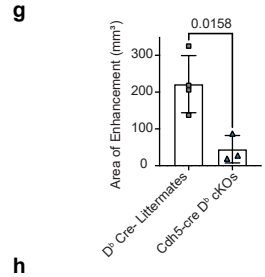
g
Area of Enhancement (mm³)
300
200
100
0
0.0158
Dᵇ Cre- Littermates
Cdh5-cre Dᵇ cKOs

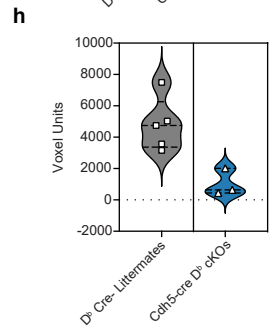
h
Voxel Units
10000
8000
6000
4000
2000
0
-2000
Dᵇ Cre- Littermates
Cdh5-cre Dᵇ cKOs

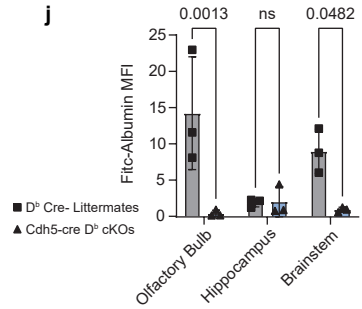
j
Fitc-Albumin MFI
25
20
15
10
5
0
0.0013
ns
0.0482
Dᵇ Cre- Littermates
Cdh5-cre Dᵇ cKOs
Olfactory Bulb
Hippocampus
Brainstem

Fig 6. Vascular leakage during PbA infection is dependent on class I molecule expression on endothelium. a) Top – Representative T1-weighted gadolinium enhanced MRI (sagittal slice) from K^b Cre- littermate day 6-8 PbA infection showing vascular leakage in regions of enhancement. Bottom - Representative T1-weighted gadolinium enhanced MRI (sagittal slice) from Cdh5-cre K^b cKO mice day 6-8 PbA infection with no vascular leakage or enhancement noted. Top right – 3D volumetric modeling of whole brain with vascular leakage highlighted in red. Top left – 3D volumetric modeling of whole brain with no apparent vascular leakage noted. b) Area measurements of regions of enhancement. Enhancement was quantified for each individual MRI slice and combined into a cumulative measurement per mouse. 2 blinded individuals performed measurements. Each data point represents the average of the scores for each mouse/scan. c) 3D pixelated volumetric measurement were obtained from all slices and averaged from 2 blinded reviewers as mentioned in b. d) FITC-albumin leakage assay results. Mice were IV injected with 66kDa FITC-conjugated albumin 1 hour prior to euthanasia to visualize regions of blood-brain barrier disruption and vascular leakage. e) Quantification of FITC-albumin mean fluorescence intensity per ROI. f) Top – Representative T1-weighted gadolinium enhanced MRI (sagittal slice) from D^b Cre- littermate day 6-8 PbA infection showing vascular leakage in regions of enhancement. Bottom - Representative T1-weighted gadolinium enhanced MRI (sagittal slice) from Cdh5-cre D^b cKO mice day 6-8 PbA infection with no vascular leakage or enhancement noted. Top right – 3D volumetric modeling of whole brain with vascular leakage highlighted in red. Top left – 3D volumetric modeling of whole brain with no apparent vascular leakage noted. g) Area measurements of regions of enhancement. Enhancement was quantified for each individual MRI slice and combined into a cumulative measurement per mouse. 2 blinded individuals performed measurements. Each data point represents the average of the scores for each mouse/scan. h) 3D pixelated volumetric measurement were obtained from all slices and averaged from 2 blinded reviewers as mentioned in g. i) FITC-albumin leakage assay results. Mice were IV injected with 66kDa FITC-conjugated albumin 1 hour prior to euthanasia to visualize regions of blood-brain barrier disruption and vascular leakage. j) Quantification of FITC-albumin mean fluorescence intensity per ROI. Data were analyzed with unpaired t test or 2way ANOVA with multiple comparisons. Violin plots and bar plots present the mean $\pm$ SD. All p-values are shown or ns for non-significant p-value *($p > 0.05$)*.

Figure 7

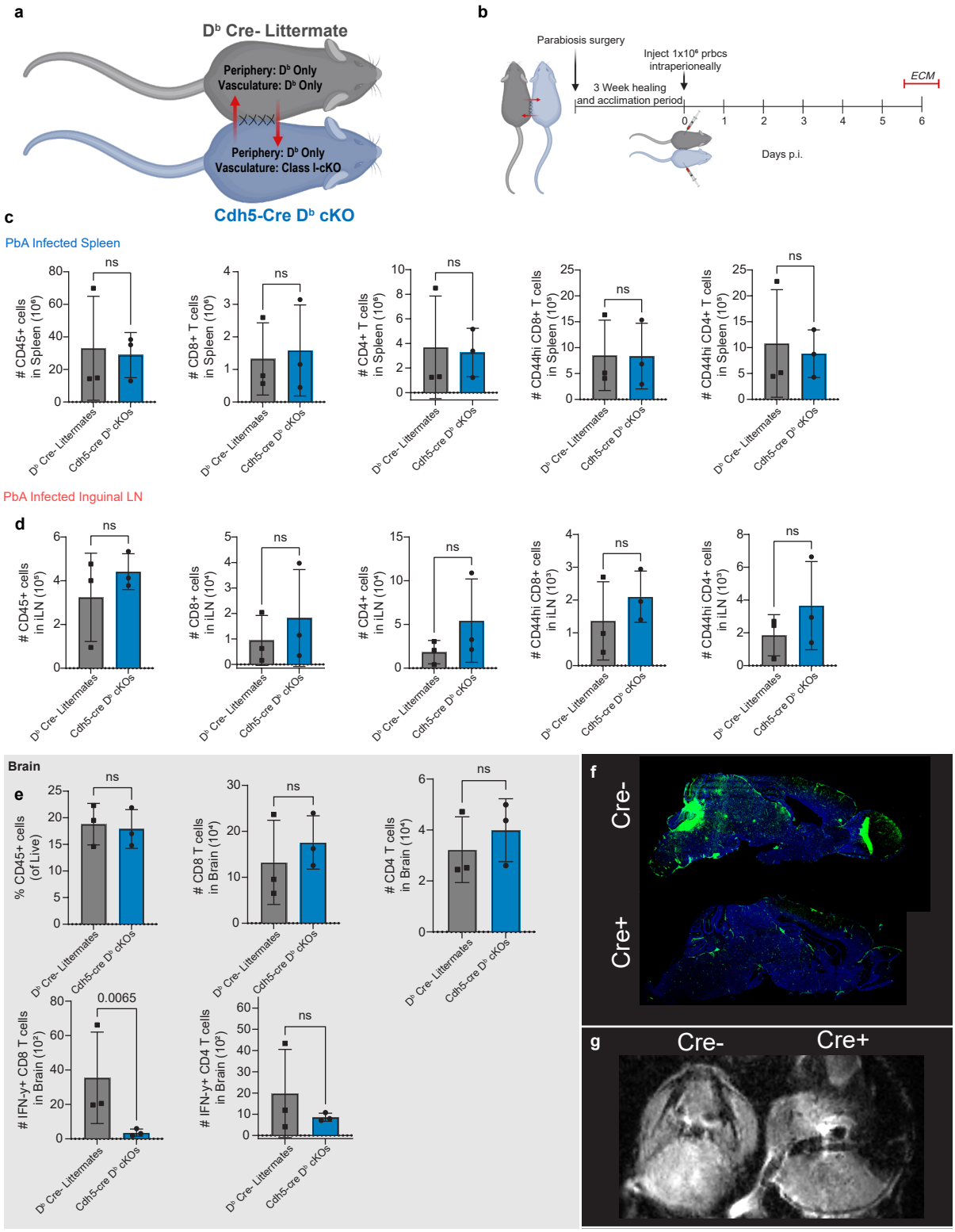
a
Dᵇ Cre- Littermate
Periphery: Dᵇ Only
Vasculature: Dᵇ Only
Periphery: Dᵇ Only
Vasculature: Class I-cKO
Cdh5-Cre Dᵇ cKO
b
Parabiosis surgery
Inject 1x10⁶ prbcs intraperioneally
3 Week healing and acclimation period
ECM
0 1 2 3 4 5 6
Days p.i.
c
PbA Infected Spleen
CD45+ cells in Spleen (10⁶)
CD8+ T cells in Spleen (10⁶)
CD4+ T cells in Spleen (10⁶)
CD44hi CD8+ T cells in Spleen (10⁵)
CD44hi CD4+ T cells in Spleen (10⁵)
ns
Dᵇ Cre- Littermates
Cdh5-cre Dᵇ cKOs
PbA Infected Inguinal LN
d
CD45+ cells in iLN (10⁵)
CD8+ cells in iLN (10⁴)
CD4+ cells in iLN (10⁴)
CD44hi CD8+ cells in iLN (10³)
CD44hi CD4+ cells in iLN (10³)
Brain
e
% CD45+ cells (of Live)
# CD8 T cells in Brain (10⁴)
# CD4 T cells in Brain (10⁴)
# IFN-γ+ CD8 T cells in Brain (10²)
# IFN-γ+ CD4 T cells in Brain (10²)
0.0065
f
Cre-
Cre+
g
Cre-
Cre+

Fig 7. PbA infected parabionts sharing peripheral circulation demonstrate requirement of endothelial D^b expression for T cell responses and development of ECM. a) Schematic depicting parabiosis procedure and respective D^b Cre- littermate and Cdh5-cre D^b cKO mice. b) Timeline of experiment depicting parabiosis surgery, healing and acclimation time and PbA infection of parabionts. c) Absolute counts of total CD45+ immune cells, CD8 T cells, CD4 T cells and activated CD8s and CD4s in the spleens of parabionts day 6 of PbA infection. d) Absolute counts of total CD45+ immune cells, CD8 T cells, CD4 T cells and activated CD8s and CD4s in the iLNs of parabionts day 6 of PbA infection. e) Absolute counts of total CD45+ immune cells, CD8 T cells, CD4 T cells and IFN-γ producing CD8s and CD4s in the brains of parabionts day 6 of PbA infection. f) FITC-albumin was IV injected one hour before euthanasia of PbA infected parabionts. D^b Cre- littermate and Cdh5-cre D^b cKO parabiont brains are visualized with FITC leakage in green. g) T1-weighted gadolinium enhanced dual MRI of parabiont pair was performed. Representative image is one axial slice with visualization of gadolinium enhancement. Data were analyzed with unpaired t test. Bar plots present the mean $\pm$ SD. All p-values are shown or ns for non-significant p-value *($p > 0.05$)*.

Figure 8

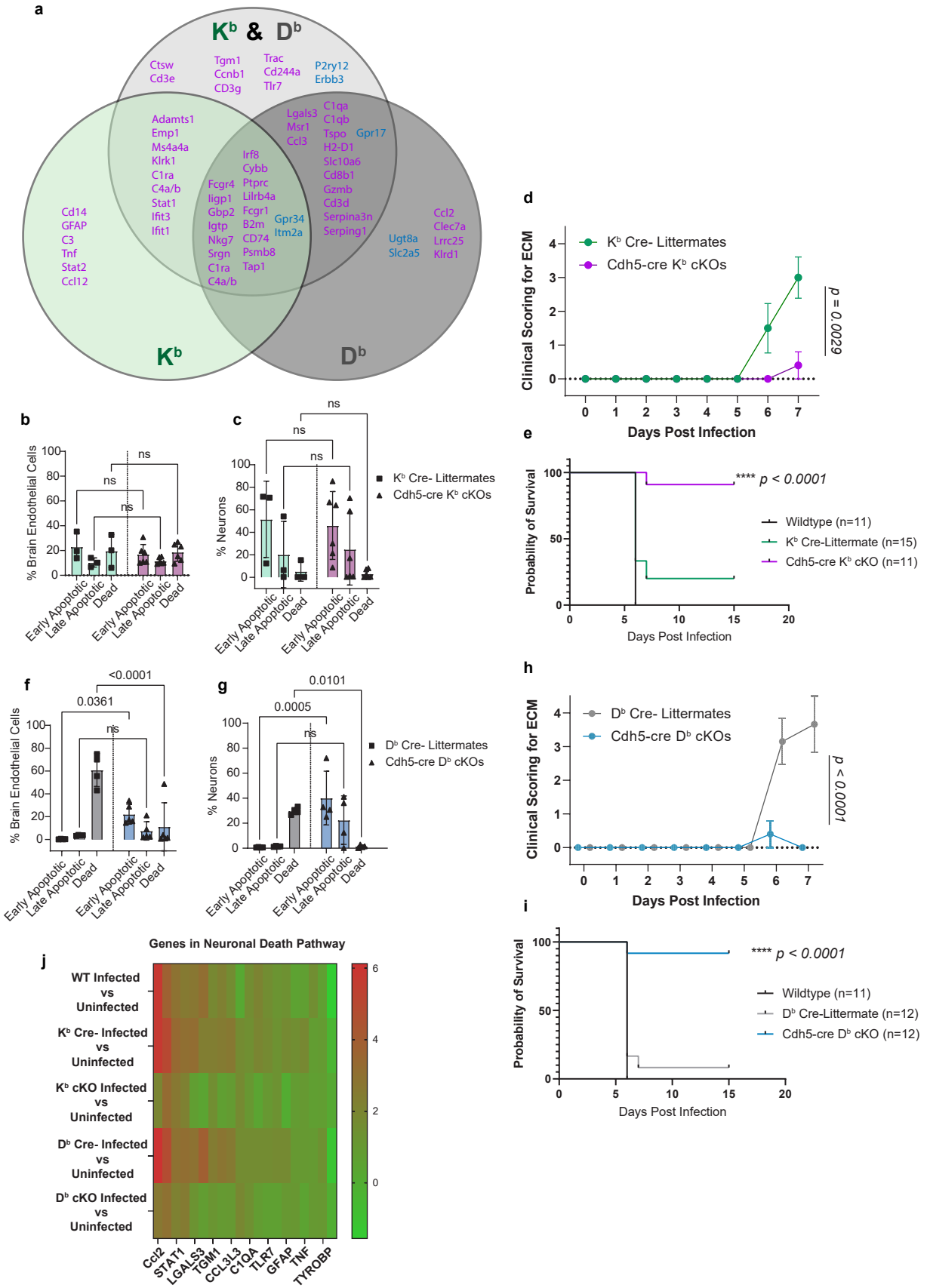
a
Kᵇ & Dᵇ
Ctsw
Cd3e
Tgm1
Ccnb1
CD3g
Trac
Cd244a
Tlr7
P2ry12
Erbb3
Adamts1
Emp1
Ms4a4a
Klrk1
C1ra
C4a/b
Stat1
Ifit3
Ifit1
Lgals3
Msr1
Ccl3
C1qa
C1qb
Tspo
Gpr17
H2-D1
Slc10a6
Cd8b1
Gzmb
Cd3d
Serpina3n
Serping1
Irf8
Cybb
Ptprc
Lilrb4a
Fcgr1
B2m
CD74
Psmb8
Tap1
Fcgr4
Iigp1
Gbp2
Igtp
Nkg7
Srgn
C1ra
C4a/b
Gpr34
Itm2a
Cd14
GFAP
C3
Tnf
Stat2
Ccl12
Ugt8a
Slc2a5
Ccl2
Clec7a
Lrrc25
Klrd1
Kᵇ
Dᵇ
b
% Brain Endothelial Cells
ns
Early Apoptotic
Late Apoptotic
Dead
c
% Neurons
Kᵇ Cre- Littermates
Cdh5-cre Kᵇ cKOs
d
Clinical Scoring for ECM
Kᵇ Cre- Littermates
Cdh5-cre Kᵇ cKOs
p = 0.0029
Days Post Infection
e
Probability of Survival
**** p < 0.0001
Wildtype (n=11)
Kᵇ Cre-Littermate (n=15)
Cdh5-cre Kᵇ cKO (n=11)
Days Post Infection
f
% Brain Endothelial Cells
<0.0001
0.0361
ns
g
% Neurons
0.0101
0.0005
ns
Dᵇ Cre- Littermates
Cdh5-cre Dᵇ cKOs
h
Clinical Scoring for ECM
Dᵇ Cre- Littermates
Cdh5-cre Dᵇ cKOs
p < 0.0001
Days Post Infection
i
Probability of Survival
**** p < 0.0001
Wildtype (n=11)
Dᵇ Cre-Littermate (n=12)
Cdh5-cre Dᵇ cKO (n=12)
Days Post Infection
j
Genes in Neuronal Death Pathway
WT Infected vs Uninfected
Kᵇ Cre- Infected vs Uninfected
Kᵇ cKO Infected vs Uninfected
Dᵇ Cre- Infected vs Uninfected
Dᵇ cKO Infected vs Uninfected
Ccl2
STAT1
LGALS3
TGM1
CCL3L3
C1QA
TLR7
GFAP
TNF
TYROBP

Fig 8. Discrete class I molecules differentially regulate cell death and neuroinflammation in the brain during ECM. Nanostring analysis was performed on whole brain isolated RNA of PbA infected C57BL/6, K^b and D^b Cre- littermates, Cdh5-cre K^b cKO, Cdh5-cre D^b cKO and uninfected controls of each group (n = 40, n = 4 mice/group). a) Venn diagrams of differentially expressed genes are visualized for comparison of differential class I regulation by wildtype mice, mice with only K^b and mice with only D^b expression. High-dimensional spectral flow cytometry was performed using a staining panel specific for stages of cell death. Frequencies of cells positive for markers of early apoptosis, late apoptosis and necrosis (late cell death) determined by annexin V staining vs viability stain gating. b) Frequencies of respective stages of cell death in Cre- littermates and Cdh5-cre K^b cKO expressed by brain endothelial cells on day 6 PbA infection. c) Frequencies of respective stages of cell death in Cre- littermates and Cdh5-cre K^b cKO expressed by mature neurons on day 6 PbA infection. d) Blinded clinical scoring was conducted daily on Cre- littermates and Cdh5-cre K^b cKO mice infected with PbA. e) Survival studies were performed on infected Cre- littermates and Cdh5-cre K^b cKO mice. Mice with K^b deletion had largely improved survival. f) Frequencies of respective stages of cell death in Cre- littermates and Cdh5-cre D^b cKO expressed by brain endothelial cells on day 6 PbA infection. g) Frequencies of respective stages of cell death in Cre- littermates and Cdh5-cre D^b cKO expressed by mature neurons on day 6 PbA infection. h) Blinded clinical scoring was conducted daily on Cre- littermates and Cdh5-cre D^b cKO mice infected with PbA. i) Survival studies were performed on infected Cre- littermates and Cdh5-cre D^b cKO mice. Mice with D^b deletion had vastly improved survival. j) IPA analysis was performed, and gene Expression Log Ration data was plotted in heat map to visualize changes in expression between groups. Data were analyzed with unpaired t test or 2way ANOVA with multiple comparisons. For survival, Kaplan Meier curves were plotted, and Log-rank (Mantel-Cox) curve comparison was performed. Scatter plots and bar plots present the mean $\pm$ SD. All p-values are shown or ns for non-significant p-value *($p > 0.05$)*.

Supplementary Figure 1

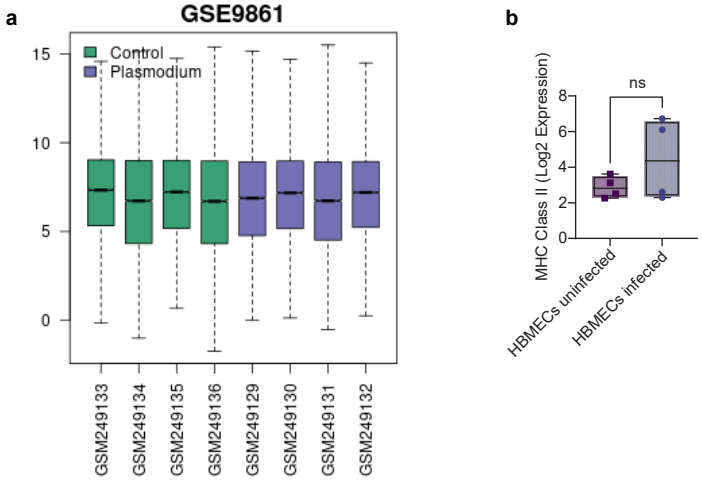

Supplementary Figure 1. Validation of human data comparison. a) Boxplots show the distribution of the expression values for each human subject. Medians are centered indicating that human datasets are suitable for comparison. Value distribution analysis performed by GEO2R Web Application – NCBI GEO. b) MHC Class II Log_2 expression in control HBMECs vs. Plasmodium exposed HBMECs. Data were analyzed with unpaired t test (b). Box plots present the mean + SD. All p-values are shown or ns for non-significant p-value *($p > 0.05$)*.

Supplementary Figure 2

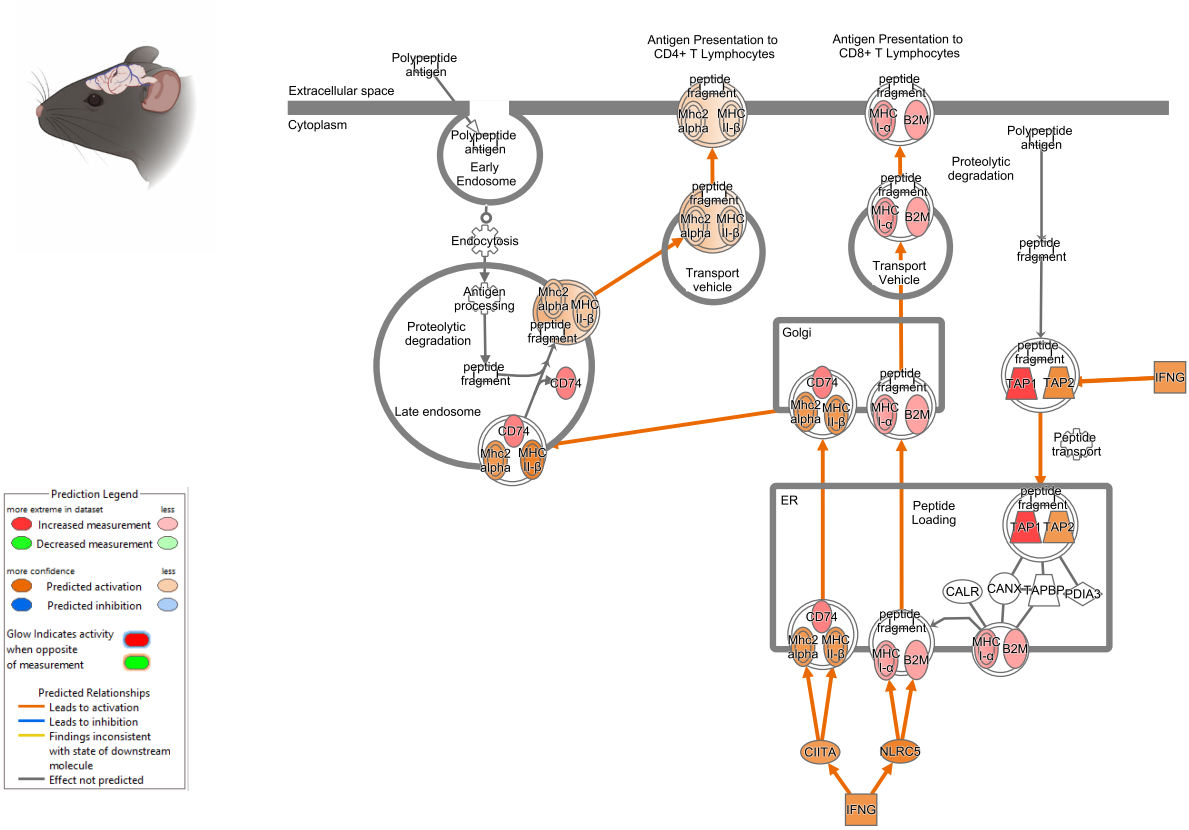

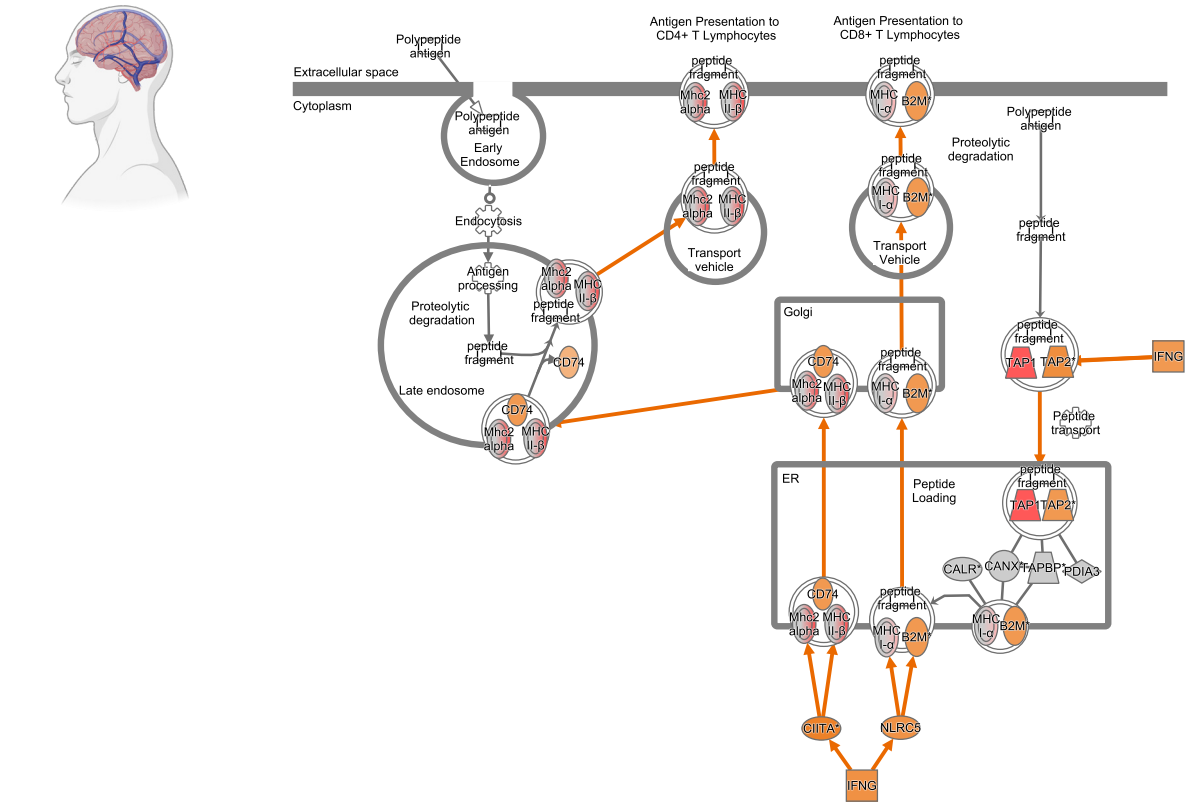

Supplementary Figure 2. Human and mouse antigen presentation pathways and corresponding genes show similar activation with *Plasmodium* infection. Ingenuity Pathway analyses of mouse and human antigen presentation pathways are depicted in schematics. Coloring of the molecules corresponds to calculated z-scores (algorithm predicting activation or inhibition). Red indicates increased gene activation, orange indicates predicted activation of pathways, green indicates decreased gene activation, blue indicates predicted inhibition of pathways, white indicates a z-score of zero with equal evidence for activation and inhibition, grey indicates that z-score could not be calculated.

Supplementary Figure 3

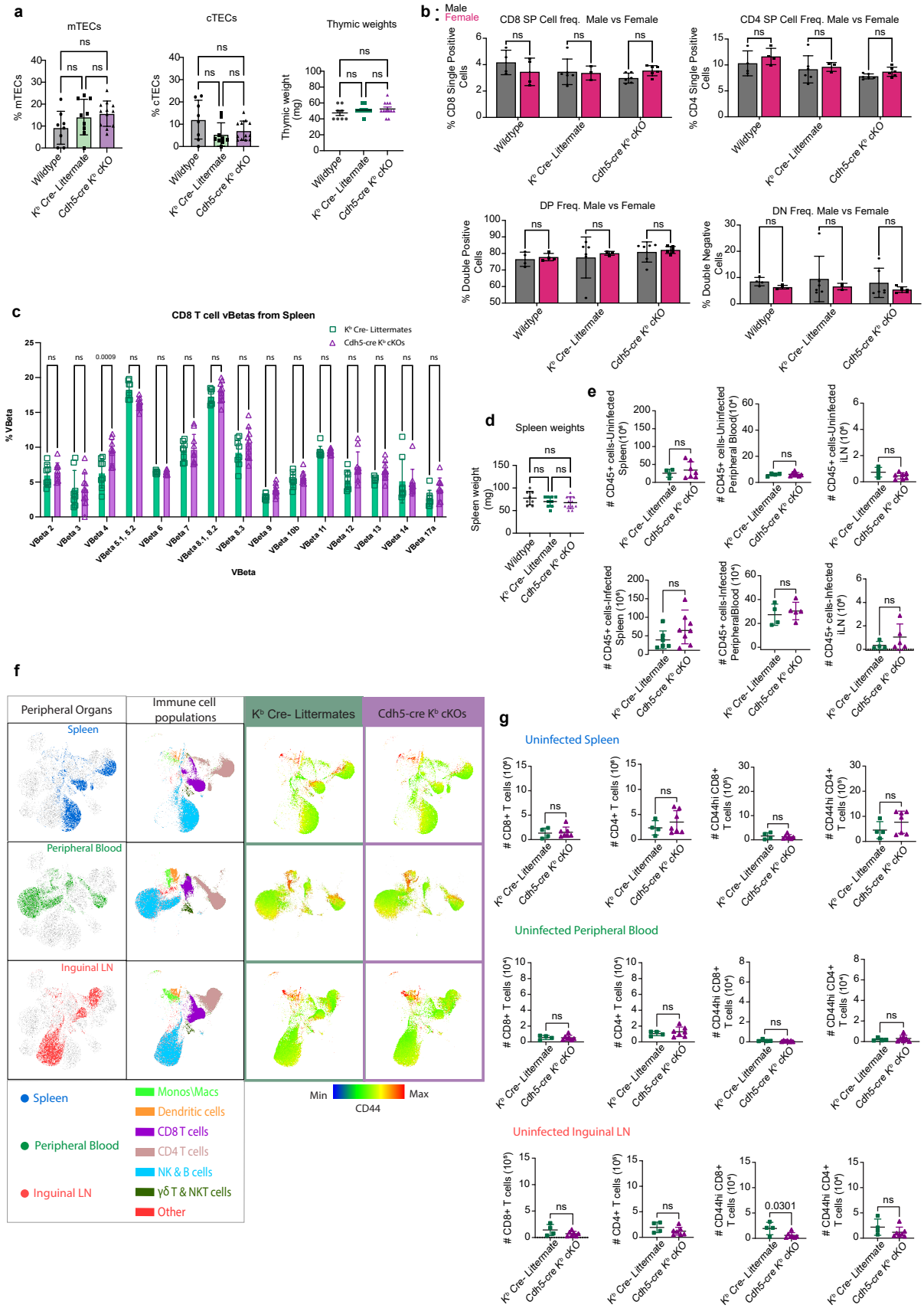

Supplementary Figure 3. Peripheral immune system is intact K^b Cre- littermates and Cdh5-cre K^b cKO mice. a) Percentage of mTECs and cTECs quantified from thymi of naïve mice across groups and thymic weights of naïve mice across groups. b) Comparison of percentages of thymic T cell subsets in males vs females across groups in naïve mice. c) Percentages of respective VBeta TCRs out of CD8 T cells of the spleen in naïve mice. d) Splenic weights of naïve mice across groups. e) Absolute counts of CD45+ immune cells in respective peripheral organs of infected and naïve mice. f) Representative UMAPs depicting peripheral organs and immune cell populations and respective heats maps with CD44 activation marker expression. g) The scatter plots show quantified absolute cell counts of CD8 T cells, CD4 T cells and CD44hi CD8 T cells and CD4 T cells in the respective organs depicted in UMAPs. Data were analyzed with unpaired t test, Ordinary 1way ANOVA with multiple comparisons or 2way ANOVA with multiple comparisons. Scatterplots and bar plots present the mean $\pm$ SD. All p-values are shown or ns for non-significant p-value *($p > 0.05$)*.

Supplementary Figure 4

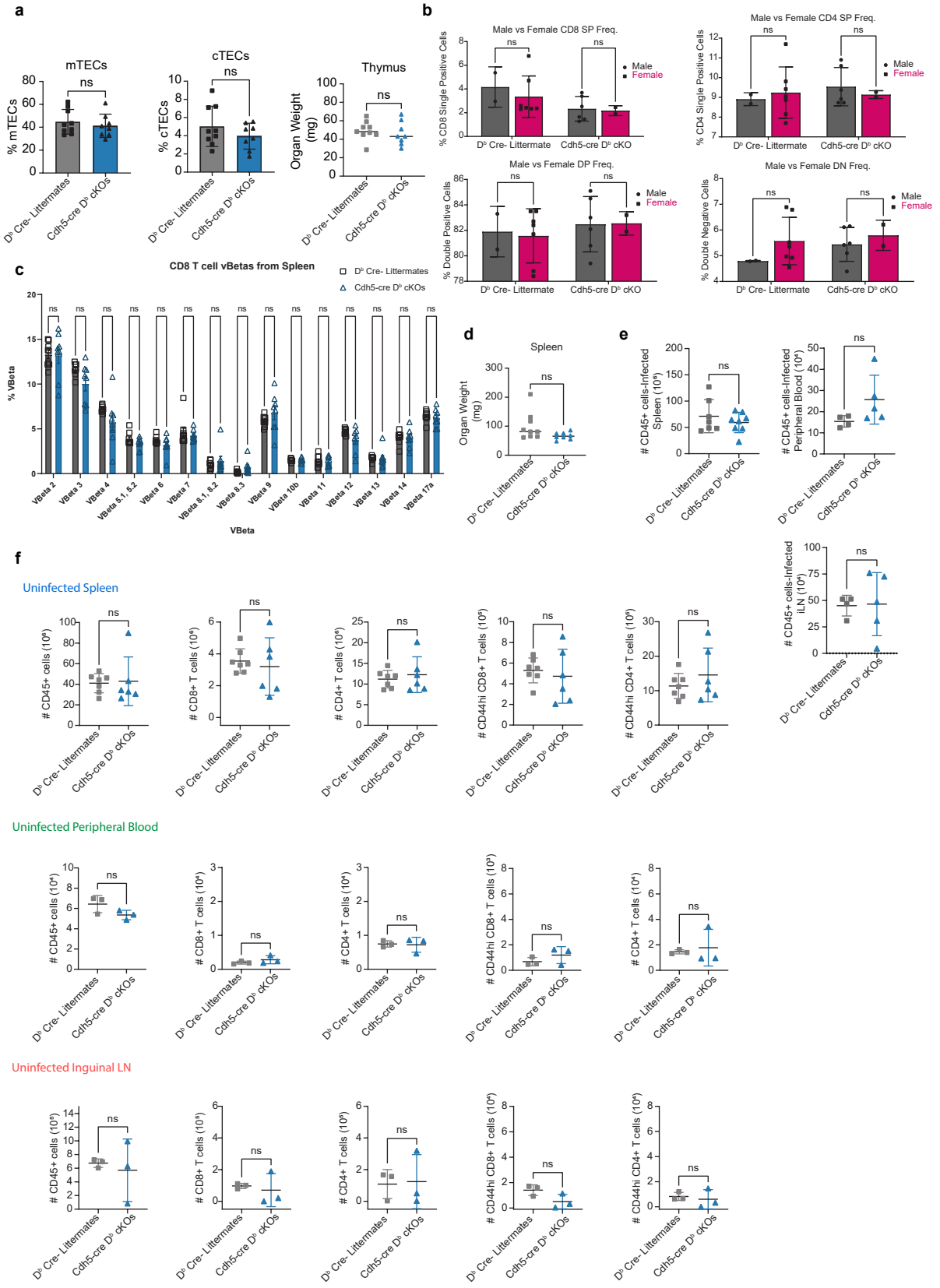

Supplementary Figure 4. Peripheral immune system is intact in D^b Cre- littermates and Cdh5-cre D^b cKO mice. a) Percentage of mTECs and cTECs quantified from thymi of naïve mice across groups and thymic weights of naïve mice across groups. b) Comparison of percentages of thymic T cell subsets in males vs females across groups in naïve mice. c) Percentages of respective VBeta TCRs out of CD8 T cells of the spleen in naïve mice. d) Splenic weights of naïve mice across groups. e) Absolute counts of CD45+ immune cells in respective peripheral organs of infected mice. f) Scatter plots show quantified absolute cell counts of CD45+ immune cells, CD8 T cells, CD4 T cells and CD44hi CD8 T cells and CD4 T cells in respective organs of naïve mice. Data were analyzed with unpaired t test, Ordinary 1way ANOVA with multiple comparisons or 2way ANOVA with multiple comparisons. Scatterplots and bar plots present the mean $\pm$ SD. All p-values are shown or ns for non-significant p-value *($p > 0.05$)*.

Supplementary Figure 5

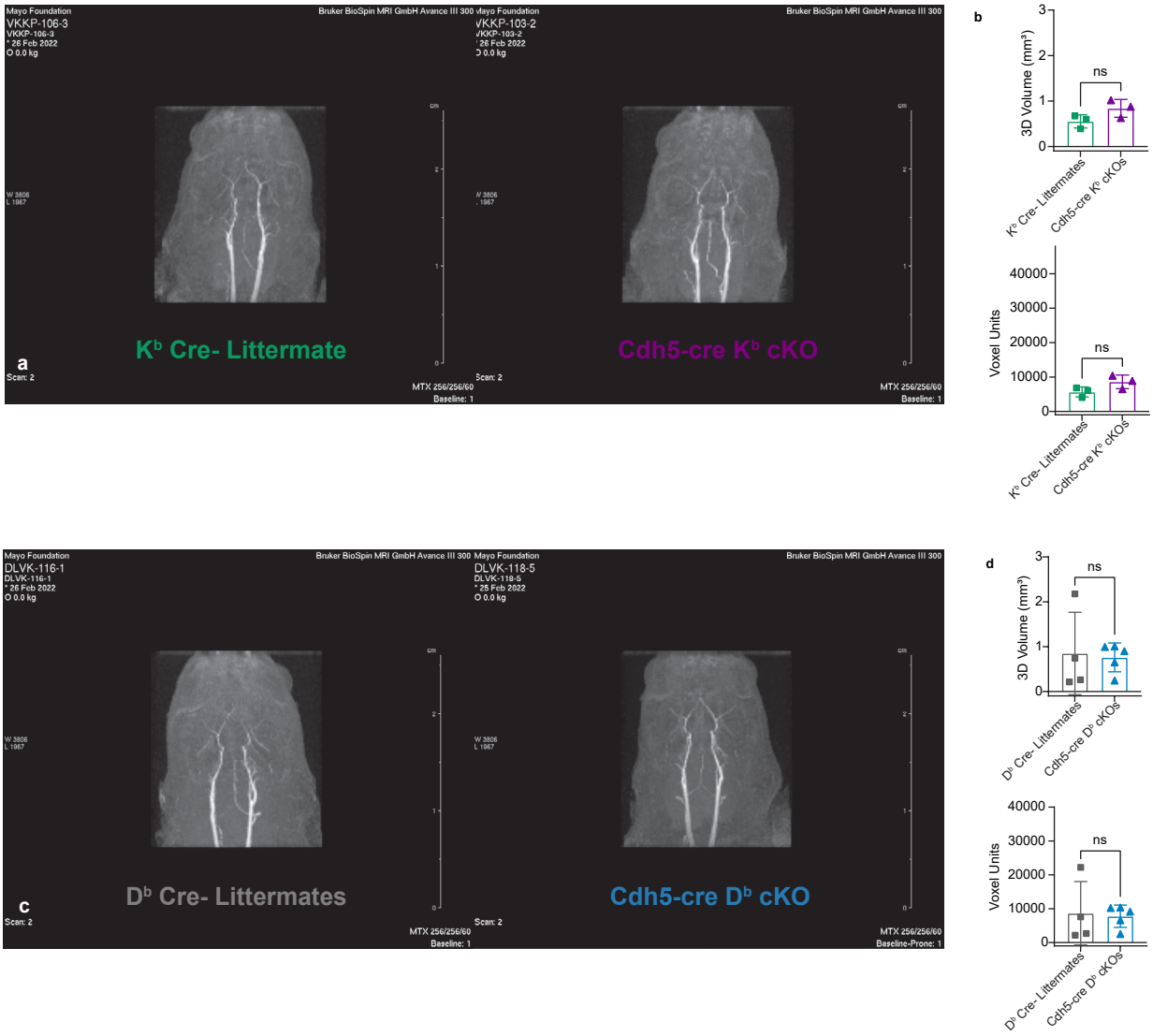

Supplementary Figure 5. No changes to brain vasculature at baseline in mice with class I deletion on endothelium. a) Representative images from maximum intensity projections (MIPs) of naïve Cdh5-Cre K^b cKO and Cre- littermate controls. Mice were IP injected with gadolinium 15 min. before MRIs were performed. b) Quantification of 3D volume of overall brain vasculature enhancement and quantification of 3D pixelated voxel units. c) Representative images from maximum intensity projections (MIPs) of naïve Cdh5-Cre D^b cKO and Cre- littermate controls. Mice were IP injected with gadolinium 15 min. before MRIs were performed. d) Quantification of 3D volume of overall brain vasculature enhancement and quantification of 3D pixelated voxel units. Data were analyzed with unpaired t test. Scatterplots present the mean + SD. All p-values are shown or ns for non-significant p-value *($p > 0.05$)*.

Supplementary Figure 6

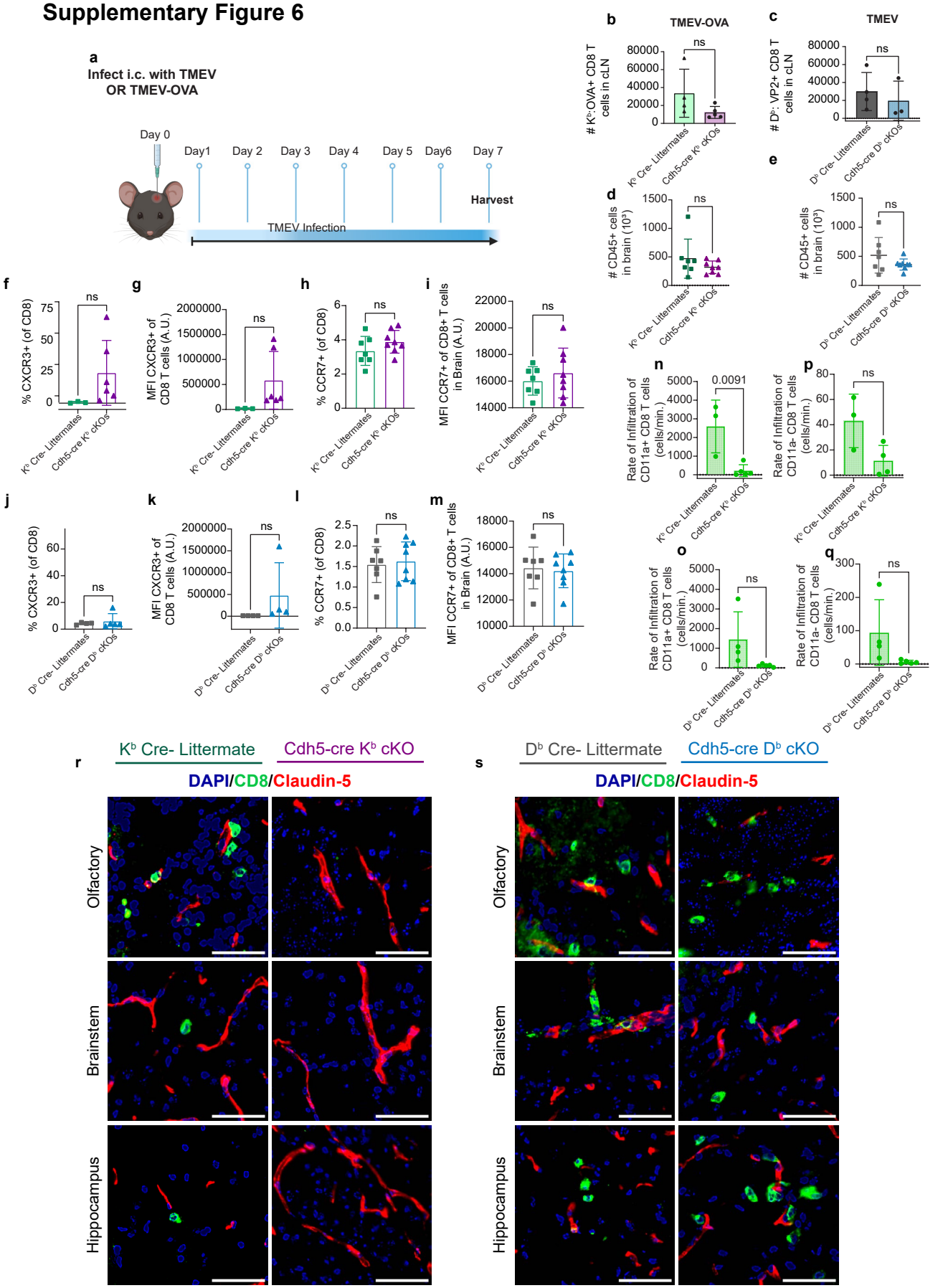

Supplementary Figure 6. CD8 T cells infiltrate regions of interest except when K^b is ablated from vasculature. a) Timeline depicting intracranial infection on Day 0 with TMEV or TMEV-OVA which is allowed to progress until day 7 when brains are harvested for high-dimensional spectral flow cytometry. b) Quantification of absolute counts of K^b: $OVA_{257-264}^+$ CD8 T cells in Cdh5-Cre K^b cKO and Cre- littermate cLNs day 7 of TMEV-OVA infection. c) Quantification of absolute counts of D^b: $VP2^+$ CD8 T cells in Cdh5-Cre K^b cKO and Cre- littermate cLNs day 7 of TMEV infection. d) Absolute counts of CD45+ immune cells in the brains of Cdh5-Cre K^b cKO and Cre- littermate brains during ECM. e) Absolute counts of CD45+ immune cells in the brains of Cdh5-Cre D^b cKO and Cre- littermate brains during ECM. f) Quantified percentage of CD8s that are CXCR3+ in brains of Cdh5-Cre K^b cKO and Cre- littermates during ECM. g) Quantification of median fluorescence intensities of CXCR3 on CD8 T cells in the brains of Cdh5-Cre K^b cKO and Cre- littermates during ECM. h) Quantified percentage of CD8s that are CCR7+ in brains during ECM. i) Quantification of median fluorescence intensities of CCR7 on CD8 T cells in the brain during ECM. j) Quantified percentage of CD8s that are CXCR3+ in brains of Cdh5-Cre D^b cKO and Cre- littermates during ECM. k) Quantification of median fluorescence intensities of CXCR3 on CD8 T cells in the brains of Cdh5-Cre D^b cKO and Cre- littermates during ECM. l) Quantified percentage of CD8s that are CCR7+ in brains during ECM. m) Quantification of median fluorescence intensities of CCR7 on CD8 T cells in the brain during ECM. n) Calculation of rate of infiltration of antigen-experienced CD11a+ CD8 T cells into the brain from IV labeled vasculature, measured in cells/min in infected K^b Cre- littermates and Cdh5-Cre K^b cKOs. o) Calculation of rate of infiltration of antigen-experienced CD11a+ CD8 T cells into the brain from IV labeled vasculature, measured in cells/min in infected D^b Cre- littermates and Cdh5-Cre D^b cKOs. p) Calculation of rate of infiltration of CD11a- CD8 T cells that have not encountered cognate peptide:MHC into the brain from IV labeled vasculature, measured in cells/min in infected K^b Cre- littermates and Cdh5-Cre K^b cKOs. q) Calculation of rate of infiltration of CD11a- CD8 T cells that have not encountered cognate peptide:MHC into the brain from IV labeled vasculature, measured in cells/min in infected D^b Cre- littermates and Cdh5-Cre D^b cKOs. Confocal imaging was performed. All images were acquired at 20X and zoomed in to 400X using FIJI. r) Representative immunofluorescence images of CD8 T cell infiltration in ROIs affected by ECM showing infiltration into these regions in the K^b Cre- littermates but not in the Cdh5-Cre K^b cKOs. Scale bar, 50 µM. s) Representative immunofluorescence images of CD8 T cell infiltration in ROIs affected by ECM showing infiltration into these regions in the D^b Cre- littermates and in the Cdh5-Cre D^b cKOs. Scale bar, 50 µM. Data were analyzed with unpaired t test. Bar plots present the mean $\pm$ SD. All p-values are shown or ns for non-significant p-value *($p > 0.05$)*.

Supplementary Figure 7

a

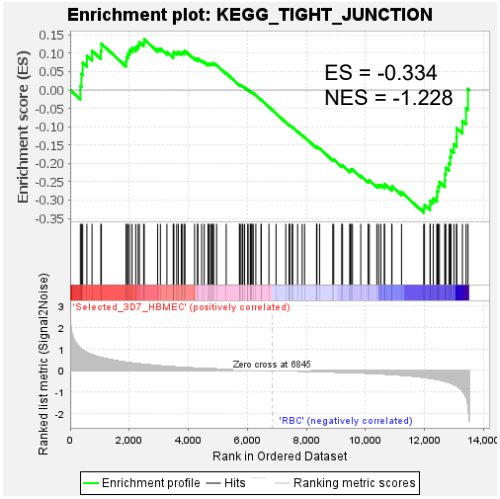

b

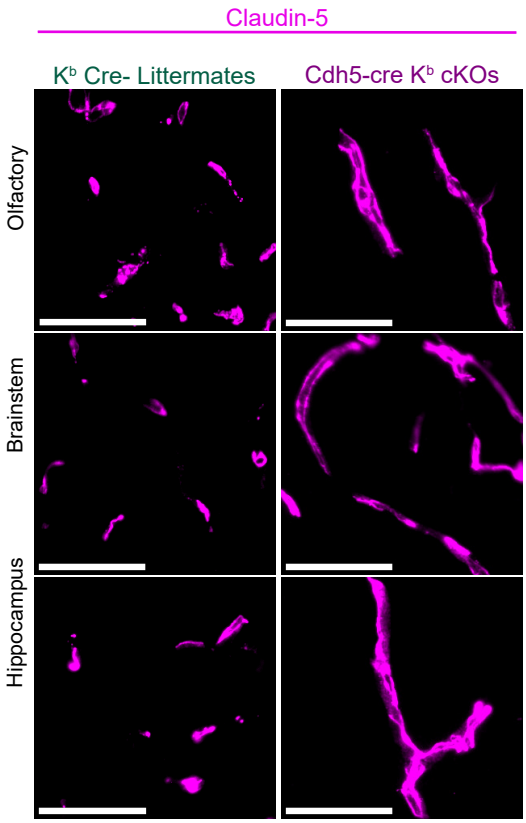

c

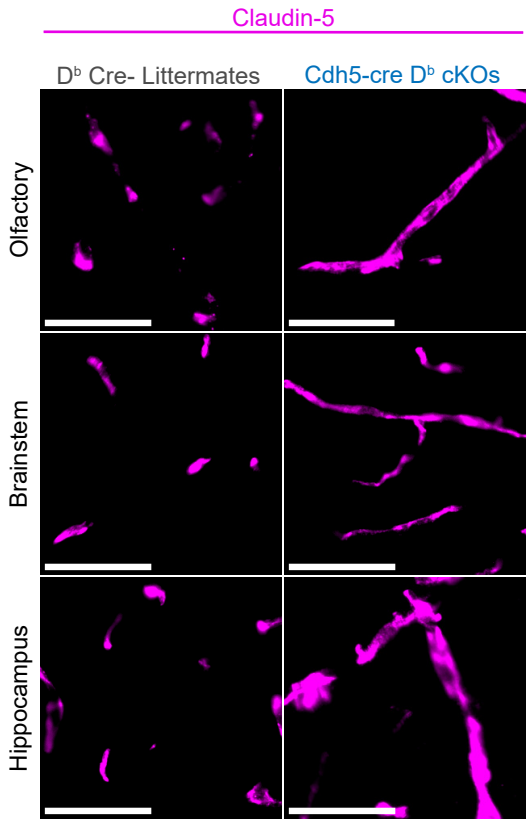

Supplementary Figure 7. Tight junction protein alterations occur in human and mice with cerebral malaria. GSEA was performed on HBMEC transcriptomic data. a) Enrichment plot showing a negative enrichment (downregulation) of molecular signature for tight junction gene set. The y-axis represents enrichment score (ES) and on the x-axis are genes (vertical black lines) represented in gene sets. The green line connects points of ES and genes. ES is the maximum deviation from zero as calculated for each gene going down the ranked list and represents the degree of over-representation of a gene set at the top or the bottom of the ranked gene list. The colored band at the bottom represents the degree of correlation of genes with the phenotype (red for positive and blue for negative correlation). Significance threshold set at nominal p-value < 0.05. Gene sets for tight junctions were significantly negatively enriched indicating downregulation in HBMECs during infection. Confocal imaging was performed. All images were acquired at 20X and zoomed in to 300X using FIJI. b) Immunofluorescence staining of tight junction protein Claudin-5 in ROI in PbA infected Cdh5-Cre K^b cKOs and K^b Cre- littermates brains day 6. Scale bar, 50 µM. c) Immunofluorescence staining of tight junction protein Claudin-5 in ROI in PbA infected Cdh5-Cre D^b cKOs and D^b Cre- littermates day 6. Scale bar, 50 µM.

Supplementary Figure 8

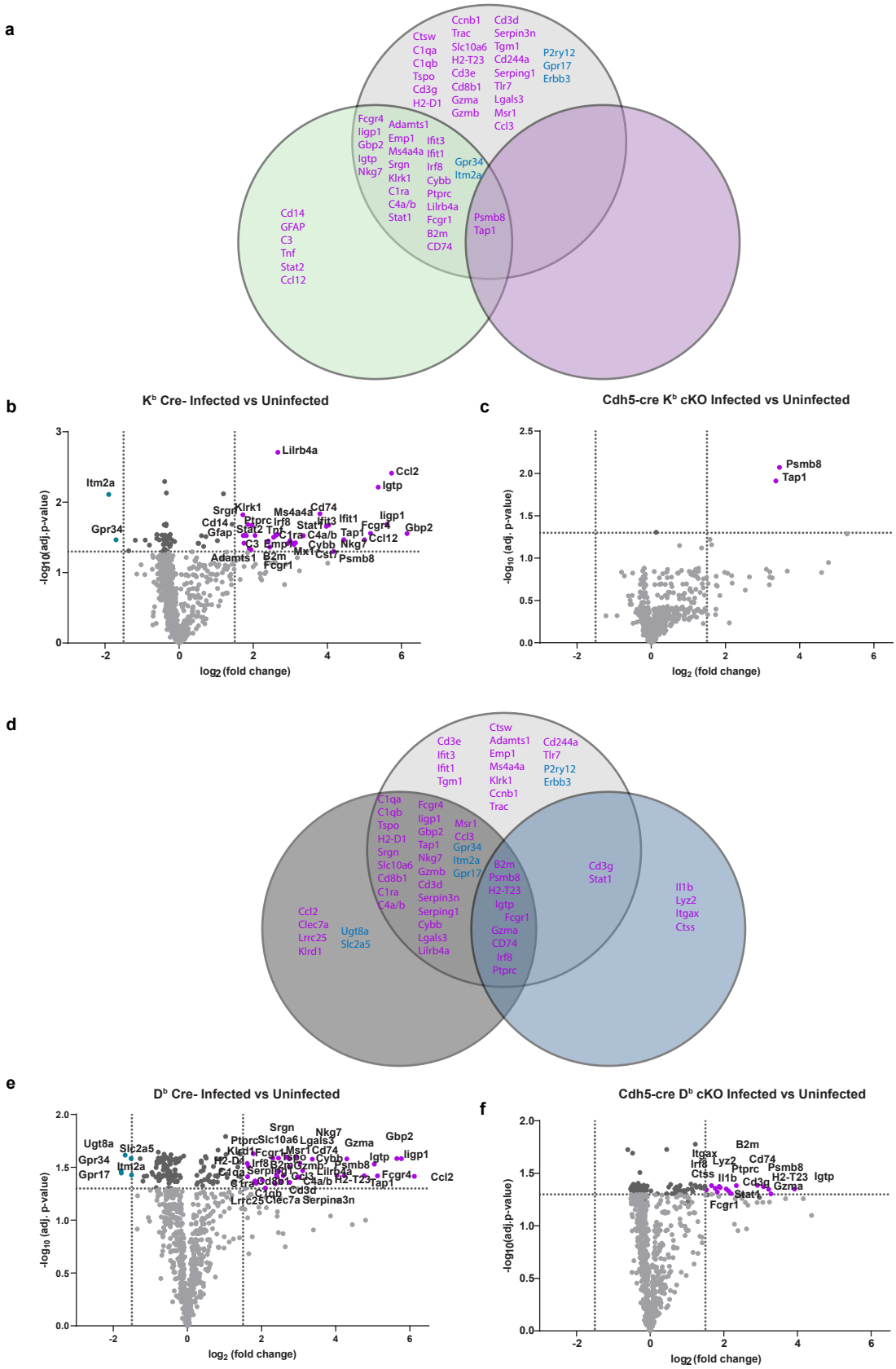

Supplementary Figure 8. Discrete endothelial class I molecules regulate differential downstream gene expression. a) Venn diagrams of differentially expressed genes are visualized for comparison of differential class I regulation in wildtype, K^b Cre- littermates and Cdh5-cre K^b cKO mice. Volcano plots of differentially expressed genes in whole brains of uninfected versus PbA infected groups of mice at endpoint during ECM. Significantly upregulated genes are indicated on upper right (purple dots). Significantly downregulated genes are indicated on upper left (turquoise dots). Horizontal dotted line indicates cutoff of adjusted p-values (-Log10 of adjusted p-value 1.3 corresponding to a threshold of p-value of 0.05). Vertical dotted line indicates cutoff of log2 Fold change (-1.5 to 1.5). b) Volcano plots of differentially expressed genes in infected K^b Cre- littermates vs Uninfected K^b Cre- littermates. c) Volcano plots of differentially expressed genes in infected Cdh5-cre K^b cKO mice vs Uninfected Cdh5-cre K^b cKO mice. d) Venn diagrams of differentially expressed genes are visualized for comparison of differential class I regulation in wildtype, D^b Cre- littermates and Cdh5-cre D^b cKO mice. e) Volcano plots of differentially expressed genes in infected D^b Cre- littermates vs Uninfected D^b Cre- littermates. f) Volcano plots of differentially expressed genes in infected Cdh5-cre D^b cKO mice vs Uninfected Cdh5-cre D^b cKO mice. P-values of overlap were adjusted using the Benjamini-Hochberg correction method.